LAWRENCE
LIVERMORE
NATIONAL
LABORATORY

LLNL-TR-812110

M4SF-20LL010302042: Process Model for Radionuclide Incorporation into Corrosion Products

E. Balboni, M. Zavarin, K. Smith, C. Booth

June 29, 2020

Disclaimer

This work performed under the auspices of the U.S. Department of Energy by Lawrence Livermore National Laboratory under Contract DE-AC52-07NA27344.

Appendix E
FCT Document Cover Sheet

Name/Title of Deliverable/Milestone	M4SF-20LL010302042: Process Model for Radionuclide Incorporation into Corrosion Products
Work Package Title and Number	SF-20LL010302041 Crystalline Disposal R&D - LLNL
Work Package WBS Number	1.08.01.03.02
Responsible Work Package Manager	Mavrik Zavarin (Name/Signature)
Date Submitted	

Quality Rigor Level for Deliverable/Milestone	☐ QRL-1 Nuclear Data	☐ QRL-2	☐ QRL-3	☒ QRL-4 Lab-specific

This deliverable was prepared in accordance with Lawrence Livermore National Laboratory's QA program which meets the requirements of

☒ DOE Order 414.1 ☐ NQA-1-2000

This Deliverable was subjected to:

☒ Technical Review

Technical Review (TR)

Review Documentation Provided

☐ Signed TR Report or,
☐ Signed TR Concurrence Sheet or,
☒ Signature of TR Reviewer(s) below

☐ Peer Review

Peer Review (PR)

Review Documentation Provided

☐ Signed PR Report or,
☐ Signed PR Concurrence Sheet or,
☐ Signature of PR Reviewer(s) below

Name and Signature of Reviewers

Brian L. Anderson Brian Anderson

Gregory Pope Gregory Pope

*Note: In some cases there may be a milestone where an item is being fabricated, maintenance is being performed on a facility, or a document is being issued through a formal document control process where it specifically calls out a formal review of the document. In these cases, documentation (e.g., inspection report, maintenance request, work planning package documentation or the documented review of the issued document through the document control process) of the completion of the activity along with the Document Cover Sheet is sufficient to demonstrate achieving the milestone. QRL for such milestones may be also be marked N/A in the work package provided the work package clearly specifies the requirement to use the Document Cover Sheet and provide supporting documentation.

June 15, 2020

M4SF-20LL010302042: Process Model for Radionuclide Incorporation into Corrosion Products

E. Balboni[1], M. Zavarin[1], K. Smith[2], C. Booth[2]

[1] Glenn T. Seaborg Institute, Physical & Life Sciences, Lawrence Livermore National Laboratory, 7000 East Avenue, Livermore, CA 94550, USA.
[2] Lawrence Berkeley National Laboratory, One Cyclotron Road, Mailstop 70A1150, Berkeley, CA 94720 USA

Contents

1. Introduction 1

2. Summary of paper "Plutonium fate during ferrihydrite to goethite recrystallization" (to be submitted by June 2020) 2

3. Magnetite coprecipitation with plutonium: preliminary results 7

4. Technetium interactions with iron oxide minerals 10

4.1. Technetium inventory 10
4.2. Oxidation state 10
4.3. Precipitation of Tc compounds and their solubility 11
4.4. Strategies for Tc disposal 13
4.5. Technetium sorption processes: adsorption and coprecipitation 13
4.5.1. Technetium adsorption studies 13
4.5.2. Technetium coprecipitation studies 14
4.5.3. Tc coprecipitation process with Fe(II) and Fe(II)/Fe(III) oxy-hydroxides 16
4.5.4. Tc coprecipitation process with Fe(II) containing sulfides and silicates 17
4.5.5. Tc coprecipitation process with Fe(III) minerals 18

5. Selenium interactions with Fe oxide minerals 19

5.1. Selenium 19
5.2. Oxidation state 19
5.3. Precipitation of Se compounds and their solubility 20
5.4. Sorption processes: adsorption, surface mediated reduction and coprecipitation 21
5.4.1. Adsorption studies 21
5.4.2. Surface mediated reduction of selenium 23
5.4.3. Coprecipitation studies 24
5.4.4. Se coprecipitation process with Fe(II) and Fe(II)/Fe(III) oxy-hydroxides 26
5.4.5. Se coprecipitation process with sulfides 26
5.4.6. Se coprecipitation process with Fe(III) minerals 27

6. Future FY21 work 28

7. Acknowledgments 28

8. References 28

1. Introduction

This progress report (Level 4 Milestone Number M4SF-20LL010302042) summarizes research conducted at Lawrence Livermore National Laboratory (LLNL) within the Crystalline Activity Number SF-20LL010302041. The research is focused on actinide and radionuclide sequestration in steel corrosion products.

Fuel matrix degradation models suggest that the near field is likely to be reducing at the time of canister breaching, steel corrosion, and radionuclide release, but more oxidizing conditions may prevail in the far field. The incorporation of radionuclides into corrosion phases may limit the rate of radionuclide release by sequestering a portion of the radionuclide source term. For these reasons there is a need to evaluate the incorporation of Pu and other radionuclides into various Fe-oxide phases, and to understand the behavior of coprecipitated phases during mineral recrystallization processes and during re-oxidation events. Radionuclide coprecipitation with Fe minerals may impact long-term repository performance and is an ongoing research focus at Lawrence Livermore National Laboratory.

The effort described in this document is focused on identifying:

- The fate of plutonium during ferrihydrite to goethite recrystallization reported as a summary of a paper that will be submitted for publication at the end of June 2020
- Preliminary results on the coprecipitation of plutonium with magnetite and its behavior during exposure to oxidative solutions

Additionally, part of our effort for FY20 is focused on performing an assessment to identify the most critical radionuclides and data gaps associated with radionuclide interaction with corrosion products. Our goal is to summarize how radionuclides are expected to interact with Fe minerals relevant for the safety assessment of a geological repository. Upon completion of this assessment, we plan to perform supplementary experiments with radionuclides identified as playing a central role in repository performance assessment and to fill the knowledge gap. The radionuclides of interest include Tc, Se, Cl, I, and Np. Synthesis methods developed for Pu incorporation into oxidized and reduced iron oxide phases can be directly applied to radionuclides of specific interest to GDSA efforts. Here we report our literature review on Se and Tc interactions with various Fe minerals.

In addition to the corrosion effort, we planned to complete our analysis and modeling of Np(IV) diffusion through bentonite buffer material and provide diffusivity and retardation parameters for use in GDSA. These data are the first attempt to quantify the diffusion of the dominant Np oxidation state likely to be present under reducing repository conditions (i.e. Np(IV)). However, due to limited access to LLNL laboratories during the COVID-19 pandemic, completion of this task has been delayed and results will only become available in FY21.

2. Summary of paper "Plutonium fate during ferrihydrite to goethite recrystallization" (to be submitted by June 2020)

Authors: Enrica Balboni, Kurt F. Smith, Liane M. Moreau, Tian T. Li, Melody Maloubier, Corwin H. Booth, Annie B. Kersting, Mavrik Zavarin

KEYWORDS: Ferrihydrite, goethite, recrystallization, plutonium, x-ray absorption spectroscopy

The fate of radionuclides, including Pu, during mineral formation and recrystallization processes is still not fully understood. Gaining a detailed, mechanistic, understanding of the interactions between iron (oxy)hydroxides and Pu is key to predicting the long-term stability and mobility of Pu in the natural and engineered environment.
The goal of this paper is to assess the fate of Pu during the ubiquitous process of ferrihydrite to goethite recrystallization. We synthesized ferrihydrite with various amounts of Pu(IV) (3000, 1000 and 400 ppm) following either a coprecipitation (FH_C-3000, FH_C-1000, FH_C-400) or sorption process (FH_S-3000, FH_S-1000, FH_S-400), and then subsequently used this material to crystallize goethite (goethite samples recrystallized from Pu coprecipitated ferrihydrite: G-FH_C-3000, G-FH_C-1000, G-FH_C-400; goethite samples recrystallized from Pu sorbed ferrihydrite: G-FH_S-3000, G-FH_S-1000, G-FH_C-3000). We provide detailed extended x-ray absorption fine structure (EXAFS) spectroscopy, transmission electron microscopy (TEM) and acid leaching analysis to elucidate the nature of plutonium association with ferrihydrite and goethite.

Our results show that variations in synthetic routes have impacts on the nature of Pu associated with both the ferrihydrite precursor and the ferrihydrite recrystallization product (goethite). When a Pu containing solution is added to a ferrihydrite mineral (sorption route), a fraction of the Pu precipitates as PuO_2 nanoparticles and the remaining Pu fraction forms a complex on the mineral surface. After hydrothermal alteration to goethite, the PuO_2-like nanoparticles are preserved while a fraction of Pu is still present as a surface adsorbed species on the goethite mineral surface (Table 1, Figure 1). There is evidence that this adsorbed species is more weakly bound to goethite than to ferrihydrite, as evidenced by a decrease in the number of Pu-Fe scatterers identified in the respective sample (the LIII-edge EXAFS data and fit results for selected samples are reported in Figures 2 and 3). This observation suggests that Pu adsorbed to ferrihydrite may be mobilized during the recrystallization processes. The analysis of the supernatant after hydrothermal alteration of ferrihydrite to goethite showed a small increase in Pu concentration confirming that some Pu re-mobilization occurs during the mineral recrystallization process.

When ferrihydrite is precipitated directly from a solution containing Fe and Pu (coprecipitation route), no PuO_2-like nanoparticles are observed (Table 1). Although it is difficult to identify the exact nature of Pu in the sample due to a high degree of disorder, there is evidence that Pu is strongly bound to the ferrihydrite solids through a combination of adsorption and/or coprecipitation as evidenced by the high number of Pu-Fe scatterers. In this sample, a fraction of Pu could coprecipitate with ferrihydrite and/or

form a polynuclear inner sphere complex. The EXAFS data show that the Pu binding site changes significantly during ferrihydrite recrystallization to goethite, indicating that Pu is mobilized during hydrothermal alteration. However, only a small fraction of Pu in the highest Pu concentration sample (G-FH_C-3000) is remobilized to form PuO_2. In the lower concentration goethite samples (G-FH_C-1000, G-FH_C-400) Pu is strongly sorbed (either coprecipitated and/or adsorbed as inner sphere complex) to the goethite as evidenced by the high number of Pu-Fe scatterers, and PuO_2 is not observed. The acid leaching results support this conclusion by showing that less Pu is accessible to leaching in goethite formed via coprecipitation process, compared to the goethite formed via the sorption process. These observations confirm that that the nature of Pu associated with the mineral will affects the leachability of Pu from the solids (Figure 4).

Overall the results presented in this study provide valuable new insights into Pu(IV)- iron (oxy)hydroxide interactions in the natural and engineered environment and highlight the importance of understanding the fate of radionuclides during mineral recrystallization processes.

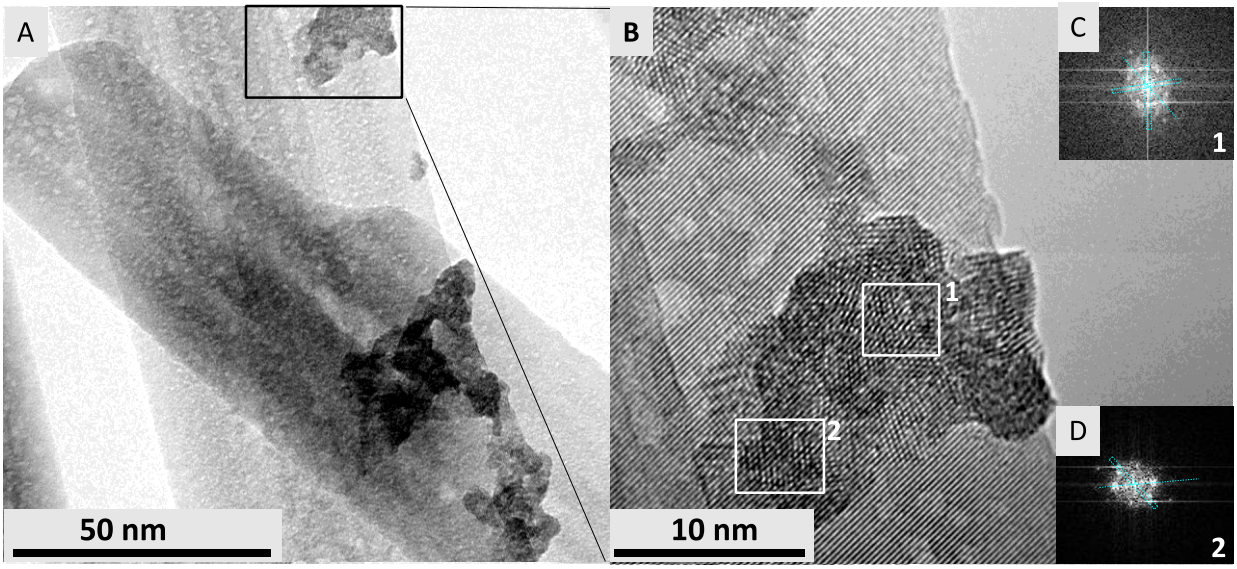

Figure 1 Pu nanoparticles on goethite G-FH_S-3000. (A) Low-magnification TEM image of large tabular goethite and intrinsic Pu nanoparticles (black inlet). (B) HRTEM image of Pu nanoparticles on goethite surface from inlet in (A); (C) and (D) FFT of HRTEM area 1 and 2 shown in panel (B), is consistent with the *fcc*, PuO_2 structure.

Table 1 Summary of EXAFS fits

Sample	Shell	N	R (Å)	σ^2 (Å^2)	E0 (eV)	*R* (%)
FH_S-3000	Pu-O	9(1)	2.31(1)	0.014(1)	-10.8(8)	8.0
	Pu-Fe	6(2)	3.39(1)	0.021(4)		
	Pu-Pu	3(1)	3.79(1)	0.008(1)		
FH_C-3000	Pu-O1	4.0(2)	2.41(1)	0.0053(7)*	-11.0(4)	3.5
	Pu-O2	3.0(1)	2.24(1)			
	Pu-Fe	8(1)	3.39(1)	0.023(2)		
G-FH_S-3000	Pu-O	8(1)	2.32(1)	0.010(1)	-11.4(8)	10.2
	Pu-Pu	4(1)	3.80(1)	0.003(1)		
G-FH_S-1000	Pu-O	8(1)	2.32(1)	0.008(1)	-11.7(7)	9.9
	Pu-Pu	4(1)	3.81(1)	0.001(1)		
G-FH_C-3000	Pu-O	6(1)	2.28(1)	0.013(2)	-12.6(12)	8.7
	Pu-Fe	1(1)	3.56(1)	0.003(4)		
	Pu-Pu	2(1)	3.80(1)	0.001(1)		
G-FH_C-1000	Pu-O	5(1)	2.21(1)	0.013(2)	-10.0(16)	13.3
	Pu-Fe	6(1)	3.17(4)	0.01(1)*		
	Pu-Fe	10(8)	3.49(2)			
G-FH_C-400	Pu-O	6(1)	2.20(2)	0.016(2)	-7.6(21)	12.2
	Pu-Fe	5(3)	3.19(2)	0.015(6)*		
	Pu-Fe	8(4)	3.47(2)			

* Indicates a tied σ^2 parameter (i.e. shared in two shells). N represents the coordination number assuming an amplitude reduction factor of 1; R denotes the interatomic distance; σ^2 represents the Debye Waller factor; ΔE0 represents the energy shift from the calculated energy fermi level.

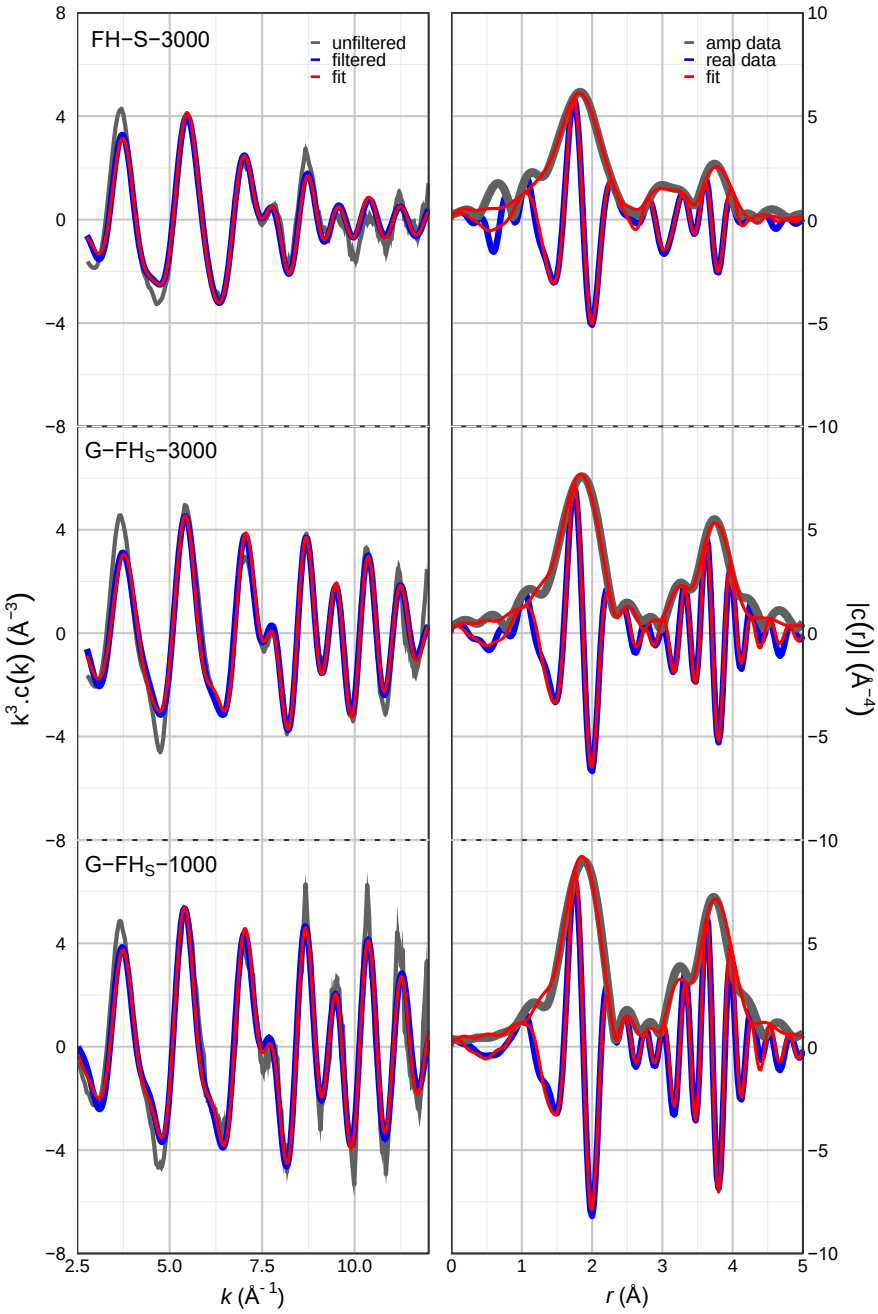

Figure 2 Pu L_{III}-edge EXAFS data and fit results for samples synthesized following the sorption method measured at 30 K. Left: Fourier transforms (FT) of the k-space data and fit. Vertical dashed lines indicate the fit range. Data were transformed between 2.5 and 12.5 $Å^{-1}$ by using a Gaussian window with a width of 0.3 $Å^{-1}$. The raw unfiltered data error bars (encompassed by the solid gray shaded area around the data set) were estimated by the standard deviation of the mean between traces. Right: EXAFS results in k-space. The filtered data and fit were back-transformed over the fit range.

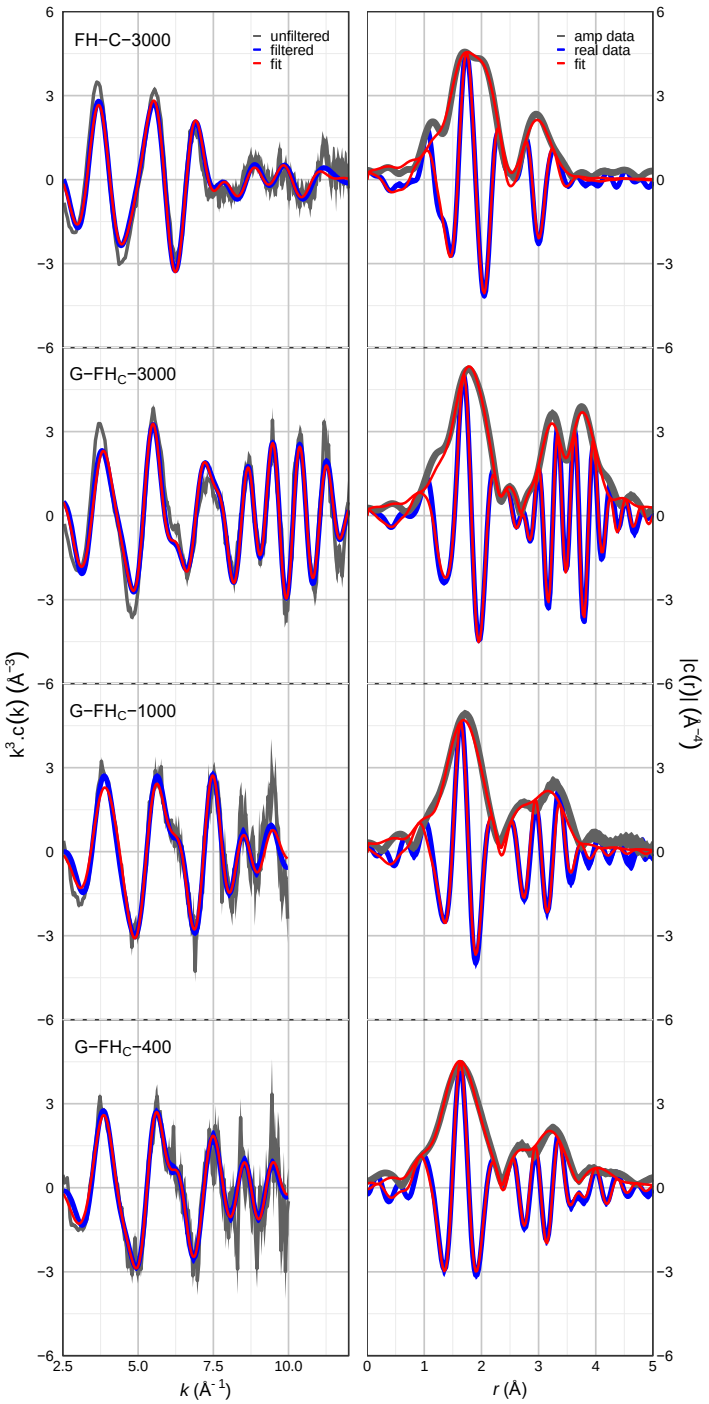

Figure 3 Pu L_{III}-edge EXAFS data and fit results for samples synthesized following the coprecipitation method measured at 30 K. Left: Fourier transforms (FT) of the k-space data and fit. Vertical dashed lines indicate the fit range. Data were transformed between 2.5 and a maximum of 12.5 $Å^{-1}$ by using a Gaussian window with a width of 0.3 $Å^{-1}$. The raw unfiltered data error bars (encompassed by the solid gray shaded area around the data set) were estimated by the standard deviation of the mean between traces. Right: EXAFS results in k-space. The filtered data and fit were back-transformed over the fit range.

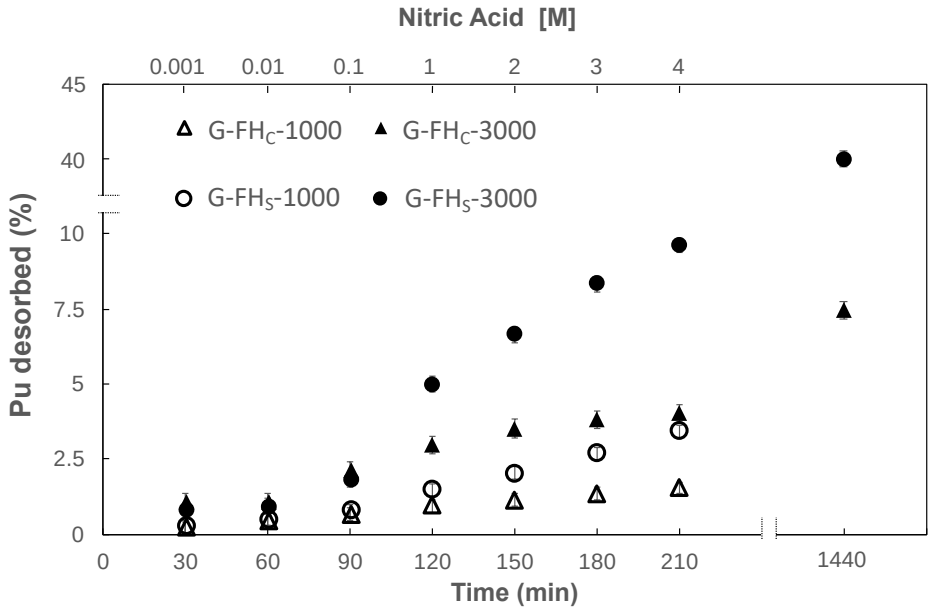

Figure 4 Leaching behavior of Pu in acidic solutions (0.001-4M) for goethite synthesized following the sorption (G-FH_S-3000, G-FH_S-1000) and coprecipitation (G-FH_C-3000, G-FH_C-1000) method. The acid leaching results show that overall more Pu is leached from goethite hydrothermally aged from ferrihydrite synthesized following the sorption than the coprecipitation method. A total of 9.6 ± 0.2% and 3.42 ± 0.3% are leached from G-FH_S-3000 and G-FH_S-1000, respectively, whereas in comparison 4.03(12)% and 1.54(8)% of Pu are leached in solution from G-FH_C-3000 and G-FH_C-1000, respectively. After 24 hours of leaching in 4 mol/L HNO_3, a total of 40(1)% of Pu is leached from G-FH_S-3000; whereas only 7.5(5)% of total Pu is leached from G-FH_C-3000.

3. Magnetite coprecipitation with plutonium: preliminary results

Pu-doped magnetite was synthesized in an anaerobic glovebox using a 0.1 M Fe(II)Cl_2 and 0.2 M Fe(III)Cl_3 prepared by dissolving the Fe salts in a degasses 0.3 M HCl solutions. An aliquot of ^{242}Pu(IV) 1.3×10^{-3} M solution was added to the Fe(III)Cl_3 solution prior to formation of any visible precipitate to achieve a Pu concentration of ~500 ppm in the solid.

The Fe(II) and Fe(III)/Pu solutions were slowly mixed on a stir plate to achieve a Fe(II)/Fe(III) molar ratio of 0.6. The pH of the mixed Fe(II)/Fe(III) solution was adjusted to ~9 using a degassed NH_4OH solution (28%v). The final product consisted of a black suspension that was left stirring for two hours in the glovebox (Mg-500). After two hours 1mL aliquot was centrifuged at 6000 rpm for 10 minutes, and results show that >99.9% Pu is associated with the solid (pH of mother liquor between 8-9). Pu aqueous concentration was measured for up to 60 days, but no significant changes were observed from the initial measurements suggesting that Pu is strongly associated to magnetite.

Aliquots of Pu-doped mineral suspensions of magnetite were rinsed from the synthetic mother liquors with degassed DI water and equilibrated with low ionic strength solution (10^{-3} mol/L $NaHCO_3$ and 5 Å~10^{-3} mol/L NaCl and pH 8) in a 0.1 g/10 mL suspension. The low ionic strength solution was degassed and stored in anaerobic conditions. Replicate samples were exposed to oxygenated atmosphere conditions and were placed on rotators. The samples were oxygenated every two days by opening the sample vials and letting the solution equilibrate with the atmosphere. After 24 hours, 7 days, 14 days and 30 days, aliquots of the mineral suspension were centrifuged (6000 rpm, 10 minutes) and the aqueous Pu in suspension was measured. After 30 days 99% of Pu remains associated with the solid.

Aliquots of as synthesized magnetite (Mg-500) and of magnetite oxidized for 30 days (Mg-500-ox) were prepared for analyses at the Stanford Synchrotron Radiation Lightsource, Stanford (CA) and preliminary results are reported below. Figure 5 shows the background subtracted EXAFS data collected on Mg-500, as well as the corresponding Fourier transform. The data were modeled (Table 2) using two shells: 10(3) O scatterers at 2.53 Å; and 6(4) Fe scatterers at 3.57 Å. Due to time constraints during data collection, the data are of low quality so results are to be interpreted carefully. However, some information can be drawn from this dataset. The Pu-O distance of 2.52(3) Å is slightly larger that Pu(III)-O as expected in Pu(III) aqueous complexes (PuIII-O aq= 2.49 Å)[1] but could be indicative of a Pu(III) complex associated with the magnetite solid. The presence of Pu-Fe scatterers suggests that this complex may be strongly bound to the magnetite surface.

Figure 6 shows the background subtracted Pu LIII-edge EXAFS and corresponding Fourier transform (FT) for Pu coprecipitated with magnetite that was subsequently oxidized for 30 days. An unconstrained fit to the data is shown in Table 2. The data could be described with a 3 shell fit. These shells consisted of 2(2) Pu-O scatterers at 1.73(3) with a σ^2 of 0.01(3) Å.[2] The second shell was with 4(1) Pu-O scatters at 2.49 Å and the final shell was fit with 6(2) Pu-Fe scatterers at 3.54 Å. There is an indication in the sample of Pu-O_{ax} scatterers strongly implying that some plutonyl species are present in this sample however due to the large error bar associated with this value we are unable to accurately quantify the extent of oxidation. Furthermore, the Pu-O and Pu-Fe interatomic distances and the number of Pu-Fe scatterers correspond to the work presented in Kirsch et al. 2011[1] who interpreted their data as Pu(III) binding to the magnetite surface in a tridentate, trinuclear complex.

Analysis of the supernatant after 30 days of oxidation experiments showed that less than 1% Pu is released to solution during 30 days oxidation, suggesting that Pu associates strongly to magnetite and is retained upon exposure to oxidative conditions.
Further efforts will need to be done to obtain higher quality x-ray absorption spectroscopy data. Increasing Pu concentration in the samples should improve data quality and reduce acquisition time.

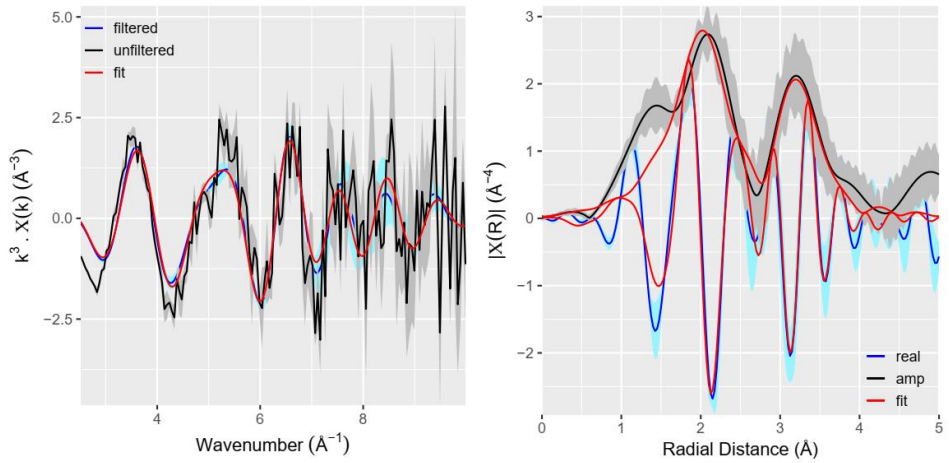

Figure 5 Left: background subtracted EXAFS collected on Mg-500. Right: corresponding Fourier transform. Fit was unconstrained.

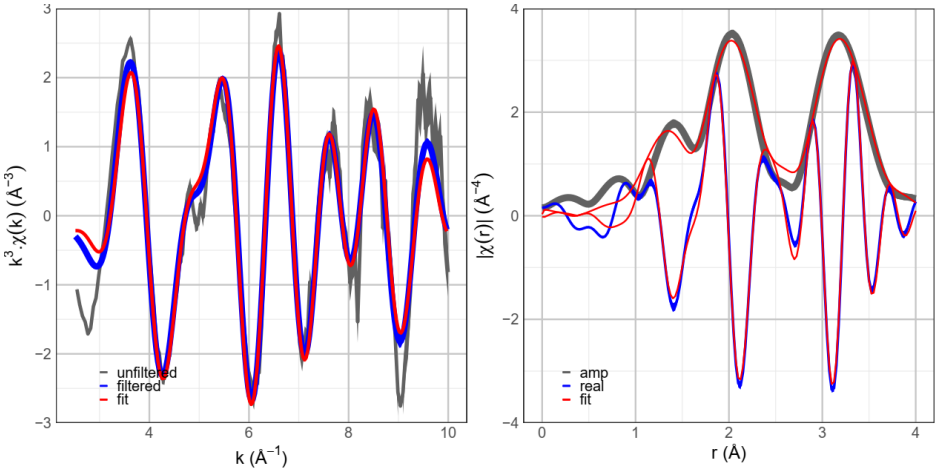

Figure 6 Pu coprecipitated with magnetite and subsequently oxidized. Left: Background subtracted Pu L_{III}-edge EXAFS. Right: Corresponding Fourier transform.

Table 2 Fitting statistics associated with Mag-500 and Mag-500-ox

Sample	**Shell**	**N**	**R(Å)**	**σ^2 ($Å^2$)**	**E0 (eV)**	***R* (%)**
Mg-500	Pu-O	10(3)	2.52(3)	0.025(6)	-8.0	16.55
	Pu-Fe	6(4)	3.57(5)	0.01(1)		
Mg-500-ox	Pu-O	2(2)	1.73(3)	0.01(3)	-3.4(17)	9.97%
	Pu-O	4(1)	2.49(2)	0.011(4)		
	Pu-Fe	6(2)	3.54(1)	0.011(3)		

4. Technetium interactions with iron oxide minerals

4.1. Technetium inventory

Technetium (^{99}Tc) is a long lived (2.1×10^5 years), high yield (6%) fission product.[2-4] Atmospheric nuclear testing resulted in ~100 to 140 TBq of ^{99}Tc released to the atmosphere, much of which has been deposited and incorporated into sediments, and ~ 1000 TBq of ^{99}Tc (1 PBq) has been released through reprocessing of spent fuel.[5] At the Hanford Site, Washington State, nearly 1990 kg of ^{99}Tc (or 1.25 PBq) was produced between 1943 and 1987 and are waiting final disposition.[6] Tc also continues to accumulate in large amounts due to active nuclear power generation with 21 kg of ^{99}Tc (13.2 TBq) produced annually in a large 1 GWe reactor.[2]

4.2. Oxidation state

Tc is a redox-sensitive element and its solubility and mobility in subsurface waters depend strongly on its oxidation state. The fundamental measurement that describes the stability of reduced and oxidized Tc is the TcO_4^- /TcO_2 couple expressed as[7]:

$$TcO_4^- + 4H^+ + 3e^- = TcO_2\,(s) + 2H_2O \qquad E_0 = 0.747 \pm 0.004 V$$

The pertechnetate anion ($^{99}TcO_4^-$) is highly soluble in aqueous solution (~11 mol/L) and occurs in oxidizing environment (>200 mV) or when exposed to the atmosphere[8]. Even in its reduced oxidation state, Tc(IV) solubility (Tc =3.08×10^{-9} M or ~5200 pCi/L; ~190 Bq/L;[7]) does not restrict Tc concentrations to below the drinking water standard of 900 pCi/L (or 5.3X10-^{10}mol/L; ~33 Bq/L [9]).

While the predominance of reducing conditions is necessary for Tc reduction, the availability of electron donors is far more critical. For example, Cui and Eriksen, 1996 [10] showed that even under conditions in which ferrous iron (Fe(II)) activity in solution was relatively high, reduction kinetics of Tc(VII) were sluggish. In contrast, when Fe(II) is sorbed onto other mineral phases, surface-mediated heterogeneous catalysis becomes important and reduction of Tc(VII) to Tc(IV) takes place rapidly above pH 6.[11-13] The rapid disproportionation of Tc in valence states between (VII) and (IV) also inhibits the reduction of Tc(VII) and hinders complete transformation to Tc(IV) unless other factors come into play, such as surface-mediated catalysis:

3Tc(V) = 2Tc(IV) + Tc(VII)
3Tc(VI) =Tc(IV) +2Tc(VII)

Overall technetium (^{99}Tc) presents unique challenges to nuclear waste disposal due to the environmental mobility of pertechnetate (TcO_4^-) under aerobic conditions.[2-4]

4.3. Precipitation of Tc compounds and their solubility

The crystalline dioxide TcO_2 and its hydrated forms ($TcO_2{\cdot}nH_2O$), crystallize as the distorted rutile structure[14] with metal-oxygen bond lengths of 1.98 Å. The initial precipitation of Tc-O compounds occurs by the formation of short (monomeric to trimeric) chains that attach to mineral surfaces under most environmentally relevant conditions (Tc $<10^{-5}$M).[15] In hydrous Tc(IV) oxide monomers and polymers, the atomic arrangement of Tc and O are different from the $TcO_2{\cdot}nH_2O$ crystals precipitated biotically or abiotically from strongly supersaturated solutions. These monomers and polymers have octahedra in an edge-sharing arrangement and a Tc-Tc distance of 2.59 Å in the chains indicating that the formation of hydrated TcO_2-type compounds with the distorted rutile configuration may occur through a complex rearrangement of these incipient molecular structures. The characterization of Tc(VII) crystalline structure is limited, however various reports show that bond lengths for the Tc(VII)-O are overall shorter (1.711 Å) than Tc(IV) compounds.[16, 17]

A number of investigators have undertaken measurements to determine the solubility of Tc(IV) in aqueous solution. Solubility determinations were made in a variety of different solutions, including natural and synthetic groundwater. Concentrations of Tc in equilibrium with hydrated TcO_2 solid compounds vary from 1×10^{-8} to 2.4×10^{-10}.[4, 7, 18-21] At pH interval between 4 and 10, the solubility depends on the nature of the substrate onto which the TcO_2 material precipitates.[7, 19-21]

The solubility of $TcO_2{\cdot}nH_2O$ was determined at high pH values (11.8 to 14.4) by Warwick et al., 2007.[22] They reported that above pH 13.5, the solubility of $TcO_2{\cdot}nH_2O$ increases linearly due likely to the formation of the $TcO(OH)_3^-$ species. The formation constant for the reaction is as follows:

$$TcO_2{\cdot}nH_2O \rightarrow TcO(OH)_3^- + H^- + (n\text{-}2)H_2O \qquad \log K_2 = -21.6$$

The presence of carbonate species in the alkaline pH range can also increase the solubility of $TcO_2{\cdot}nH_2O$ with formation of $Tc(OH)_2CO_3^0$, $Tc(OH)_3CO_3^-$, $Tc(OH)(CO_3)_2^-$, and $Tc(OH)_2(CO_3)_2^{2-}$ complexes which may increase the solubility by a factor of ~2.5-10 times.[23, 24] Increase in Tc solubility was observed in chloride solutions (1×10^{-3} to 5 M NaCl) with formation of $TcCl_6^{2-}$ and $TcCl_4^0$ complexes[25] at relatively low pH[26], and in the presence of ubiquitous natural ligands such as humic substances.[27, 28]
In experiments with relatively high concentrations of Tc ($>10^{-5}$ M Tc), investigators have reported formation of colloids of Tc at moderately acidic (pH 4) conditions[29] and in alkaline media containing high concentrations of Cl^- and SO_4^{2-}.[30] The structure of the colloid particles was revealed by EXAFS to be one-dimensional chains of Tc(IV) in octahedral coordination that connect through edge-sharing of the polyhedral.[30] The Tc-Tc distance is 2.53 Å (253 pm), and the Tc-O bond lengths alternate between short (1.80 Å) and long (1.98 Å). Tc colloids will condense from pertechnetate solutions exposed to radiolysis at acid to near-neutral pH values.[31, 32] Radiolysis caused reduction of Tc(VII) and formation of Tc(IV) polymers and colloids, first as Tc(IV), then as $TcO_2{\cdot}nH_2O$ nanoparticles as the solution pH increased.[31, 32]

The solubility of Tc(IV) is also complicated by the tendency of amorphous Tc dioxide [TcO_2(am)] to form more readily than its crystalline analog under most pH conditions. Like $TcO_2 \cdot nH_2O$ the solubility of TcO_2(am) is pH-independent from acidic to alkaline conditions, but is a factor of 10 times more soluble.[18] Further, TcO_2 solubility is strongly influenced by heterogeneous precipitation kinetics on the surfaces or within Fe(II)-bearing phases. For Tc, precipitation is usually preceded by reduction of Tc(VII) to Tc(IV) and the rate of reduction is strongly controlled not only by the form of Fe(II) (aqueous, structural, or sorbed), but also by the identity of the phase associated with reduced iron (phyllosilicates v. iron oxides and hydroxides). The ability of Fe(II) to reduce Tc(VII) therefore depends on whether Fe(II) is a dissolved species, sorbed onto mineral surfaces, or is manifested in a structural role in the mineral. Principally, Fe(II) oxide, hydroxide and sulfide phases have been reported to facilitate the precipitation of Tc(IV) compounds. Investigations have shown that TcO_2 compounds will precipitate on the surfaces of magnetite ($[Fe^{2+}Fe^{3+}]O_4$)[10, 19], goethite [α-FeO(OH)][12], ferrihydrite [$Fe(OH)_3$][11], and "green rust".[33] The relative power of Fe(II) in its various forms to reduce Tc(VII) was given by [12] in this order: Fe(II) aqueous ~ Fe(II) sorbed onto phyllosilicates << structural Fe(II) in phyllosilicates << Fe(II) sorbed onto hematite and goethite. The association of Tc(IV) with structural Fe(II) has a profound influence on the rate of re-oxidation of Tc and it is discussed in detail below. Kobayashi et al., 2013[34] investigated the reduction/sorption of Tc(VII) in the presence of Fe(II) (magnetite, mackinawite and siderite) and Fe(III) (goethite and hematite) minerals. Their results showed that Tc reduction was only observed in the presence of the Fe(II) minerals demonstrating that Tc redox behavior strongly depends on the Eh values in solution and independent of the chemicals used to fix redox conditions. A diagram illustrating the stability fields of the Tc species as a function of pH and E_h is displayed in Figure 7.

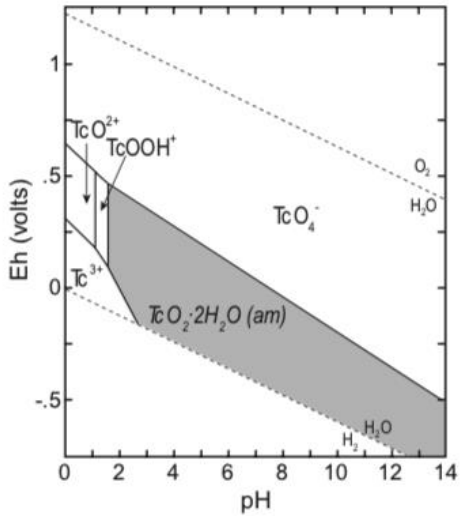

Figure 7 EH-pH diagram for Tc.[2] The shaded area represents the regions in which the amorphous solid $TcO_2 \cdot 2H_2O$ (am) is stable. Note that nearly the entire field for the species $TcO(OH)_2°$ is congruent with the stability field of $TcO_2 \cdot 2H_2O$(am).

4.4. Strategies for Tc disposal

Since the stable form of Tc under anaerobic conditions, Tc(IV), is not highly mobile the most effective method for preventing Tc migration is disposal in an anaerobic repository.[4] Another potential method for preventing Tc migration from a waste repository is stabilizing it within a durable waste form that can sequester ^{99}Tc until it has decayed. A general rule of thumb is that ten half-lives are sufficient to allow a radionuclide to decay; however, this period can be shorter or longer depending on the risks posed by the radionuclide.[35] In the U.S., all of the operational and proposed repositories for spent nuclear fuel (Yucca Mountain) and for fission products generated during plutonium production (Savannah River Site and Hanford Reservation) are aerobic and/or near-surface sites.[36-38] The disposal of ^{99}Tc in these aerobic repositories drives the interest in waste forms for ^{99}Tc that are stable in aerobic environments. Understanding sorption behavior of Tc is fundamental to determining repository performances over long period of time.

4.5. Technetium sorption processes: adsorption and coprecipitation

4.5.1. Technetium adsorption studies

Compared to the other radionuclides, much fewer sorption studies have been conducted to determine the sorption processes of Tc on mineral substrates. [39] Baston et al., 2002[18] measured Kd values for Tc(IV) sorption to Boom Clay at low Eh values (-230 mV) in conditions below the threshold of Tc(IV) reduction, and reported Kd values between 0.8 to 1.8 mL/g. In oxidizing systems, where pertechnetate is the dominant species, there is virtually no sorption of dissolved TcO_4^-. Autoradiographic analyses of rock and mineral thin sections contacted with $^{95m}TcO_4^-$ containing solutions, under oxic and anoxic conditions, have confirmed that virtually no sorption takes place in the presence of oxygen[40]. Overall the measured Kd for typical geologic materials tends to be very low (Table 3). The Kd values of $Tc(VII)O_4^-$ species onto hematit [41], magnetite and goethite, as well as goethite-coated sands [42] are < 5.4 mL/g (Table 3). Sheppard and Sheppard (1986)[43] reported low values of Kd (<0.005 mL/g) measured on soils in lysimeter tests. Elwear et al., 1992[44] measured Kd values of pertechnetate on a variety of geologic materials and reported values of ≤2 mL/g. Kaplan and Serne, 1998[45] reported small positive to negative Kd values (<0.11 mL/g) for soils sampled from the Hanford Site, Washington State, and < 0.29 mL/g for Savannah Rivers site sediments.[42] These results reflect the electrostatic repulsion between the negatively-charged pertechnetate anion (TcO_4^-) and the negative surface charge carried by sedimentary materials in temperate climates at near-neutral pH values.

Table 3 Sorption Kd of Tc onto geologic materials

Study	Solution	Geologic material	K_d (mL/g)
Kaplan, 2002; Li and Kaplan, 2012[39, 42]	Tc(VII)	Sands coated with Fe_2O_3 (pH 3.2-6.8)	0-0.3
Sheppard and Sheppard, 1986[43]	Tc VII	lysimeter	
Palmer and Meyer, 1981[41]	Tc(VII)	magnetite	5.4
Palmer and Meyer, 1981[41]	Tc(VII)	hematite	0.8
Elwear et al., 1992[44]	Tc(VII)	geologic media	<2
Kaplan and Serne, 1998[45]	Tc(VII)	Hanford sediments	<0.11
Baston et al., 2002 [18]	Tc(IV)	Boom Clay	0.8-1.8

4.5.2. Technetium coprecipitation studies

Surface sorbed Fe(II) on Fe-bearing minerals under reducing conditions can promote surface mediated reduction of Tc(VII) to Tc(IV).[12] When Tc(VII) is reduced to Tc(IV), the concentration of Tc is well above that of saturation, and surface precipitates and colloids, rather than an aqueous complex, may form. Studies have shown that during this surface mediated Tc(VII) reduction process, reduced products consists of sorbed octahedral TcO_2 monomers and dimers. In some instances x-ray absorption spectroscopy studies have shown Fe(III) in the second coordination shell of Tc, indicating that Tc may become incorporated into the structure of various Fe-bearing minerals (discussed in detail below). The similarity of the ionic radius of six-coordinate Tc(IV), 0.645 Å, to that of Fe(III), 0.645 Å, suggests that Tc(IV) can replace Fe(III) in an iron oxide provided that the difference in charge is balanced.[46] There are a few reports in the literature that address the coprecipitation behavior of Tc in Fe bearing minerals including oxides, hydroxides, sulfides and clays and results are summarized below. Tc is mostly immobile under reducing conditions[4], so the coprecipitation of Tc with minerals such as magnetite, green rust or white rust may be favored. However these Fe(II) minerals are usually not stable under aerobic conditions, and the fate of coprecipitated Tc upon exposure could be an issue of concern. Fe(III) iron oxides like α-Fe_2O_3 are unstable towards reduction; however both hematite (α-Fe_2O_3) and goethite (α-FeOOH) are well known to be stable under aerobic conditions.[47-50] Results of coprecipitation studies are summarized in Table 4 and discussed in detail in the following paragraphs.

Table 4 Summary of Tc coprecipitation studies with Fe minerals (n.d= not determined in study; b.d.l.= below detection limit as reported by cited study)

Study	**Mineral**	**Tc uptake (%)**	**Tc environment upon coprecipitation**	**Remobilized Tc (%) upon oxidation**	**Tc environment after oxidation**
Zachara et al., 2007[11]	Ferrihydrite/ magnetite pH 7-8	100	Tc(IV) dimer bound in bidentate edge-sharing mode to octahedral Fe(III)	7% Tc(VII) pH 8 over 5 days oxygenation	n.d
	Ferrihydrite/ magnetite pH 6	0	n.d	n.d	n.d
Lukens and Saslow, 2018[51]	Hematite	82	Tc(IV) replaces Fe(III) octahedral site	5% 200 days in DI water (pH ~7)	Tc(IV) replacing Fe(III) in the hematite lattice
	Magnetite	97	Tc(IV) occupies octahedral site	12% 200 days in DI water (pH ~7)	n.d
Saslow et al., 2017[52]	$Fe(OH)_2$ to magnetite (Cr co-contaminant)	99.5	$TcO_2.H_2O$; TcO_4^-, < 17(5)% Tc incorporated into magnetite	n.d	nd
Pepper et al., 2003[33]	Green rust (sulfate and carbonate) High $NaNO_3$	99.8	Tc(IV) as surface complex (monomer, dimer) in a TcO_2-like environment	n.d.	On contact with air, the green rusts oxidize to poorly crystalline goethite, but the Tc environment is unchanged
Um et al., 2011[53]	Fe(II)-goethite (some magnetite)	>93	Tc(IV) replaces Fe(III) octahedral site	<5% over 180 days	Tc(IV) incorporated within the goethite mineral lattice is resistant to re-oxidation.
Um et al., 2012[54]	Fe(II)-goethite pellets	>100	Tc(IV) replaces Fe(III) octahedral site	<1% 120 days	XANES only the Tc(IV) oxidation state
McBeth et al., 2011[55]	Bio-magnetite	100	Short range Tc(IV)O_2 like environment , possible incorporation Tc(IV) replacement in Fe(III) octahedral site	<4%	Octahedrally coordinated Tc(IV) may be incorporated into the re-oxidized mineral product;
	Bio-siderite $FeCO_3$	84	Short range Tc(IV)O_2-like environment	<6.2%	Hydrous TcO_2-like coordination environments
	Bio-vivianite $Fe_3(PO_4)_2.8H_2O$	68	Short range Tc(IV)O_2 like environment	18.7% over 45 days oxidation	Octahedrally coordinated Tc(IV) may be incorporated into the re-oxidized mineral product;
	Fe(II) gel	100	Short range Tc(IV)O_2 like environment	<4% nitrate mediated oxidation	Hydrous TcO_2-like coordination environments

Study	Mineral	Tc uptake (%)	Tc environment upon coprecipitation	Remobilized Tc (%) upon oxidation	Tc environment after oxidation
Yalçıntaş et al., 2016[56]	Magnetite	b.d.l.	Tc incorporation in Fe sites + Tc-Tc dimers sorbed	n.d.	n.d
	Mackinawite	b.d.l.	Tc-S like phase + TcO_2+H_2O (possible surface precipitates)	n.d.	n.d.
Livens et al., 2004; Wharton et al., 2000[57, 58]	Mackinawite	98	Tc(IV)S_2-like species	n.d	Tc(IV) in an oxide, rather than a sulfide environment.
Marshall et al., 2014[59]	Ferrihydrite to magnetite (pH 10.3-13)	100	Tc(IV) was predominantly incorporated into the magnetite octahedral site in all systems studied	40 over 152 days (maghemite/goethite) in CO2 free air	Tc(IV) replacing Fe(III) in the magnetite/maghemite lattice

4.5.3. Tc coprecipitation process with Fe(II) and Fe(II)/Fe(III) oxy-hydroxides

Pepper et al.[33] reported that treatment of green rust (layered hydrous oxides containing both Fe(II) and Fe(III) and with interlayer sulfate or carbonate anions) with pertechnetate results in Tc(IV) incorporation into an iron oxide phase. Green rusts concentrates >99.8% of ^{99}Tc, present as $[TcO_4]^-$, from aqueous solution, even in the presence of high concentrations of $NaNO_3$, a common constituent of radioactive waste streams.[33] The mechanism of removal from solution appears to occur through a reduction process and formation of strong Tc(IV) surface complexes.[33] X-ray absorption spectroscopy shows that $[TcO_4]^-$ is reduced by reaction with both sulfate and carbonate forms of green rusts and is found in a TcO_2-like environment. On contact with air, the green rusts oxidize to poorly crystalline goethite, but the Tc environment is unchanged. There is no increase in Tc solubility associated with oxidation of the host green rust. This behavior suggests that green rusts may be useful in restricting Tc migration from repositories.[33] Treatment of alkaline solutions (pH=13.5) containing TcO_4^- and CrO_4^{2-} with white rust, $Fe(II)(OH)_2$, results in incorporation of both transition metals into the magnetite structure.[52]

Long term exposure of magnetite ($Fe^{(II/III)}{}_3O_4$) to pertechnetate solutions results in reduction of TcO_4^- to Tc(IV), and incorporation of Tc(IV) into the crystal lattice of Fe_3O_4.[34, 56] McBeth et al., 2011[55] added pertechnetate ($Tc(VII)O_4^-$) to samples of biogenic and abiotically synthesized magnetite at low concentration and higher concentration XAS experiments. Complete removal of Tc(VII) from solution was achieved in magnetite systems. In select, higher concentration Tc XAS experiments, XANES spectra showed reductive precipitation to Tc(IV). Low concentration re-oxidation experiments with air resulted in only partial remobilization of Tc. Upon exposure to air, the Tc bound to the Fe-minerals was resistant to oxidative remobilization. The resultant XANES spectra of the re-oxidized minerals showed Tc(IV)-like spectra in the re-oxidized Fe-phases. In this system Tc is largely recalcitrant to re-oxidation over medium-term timescales and there is

spectroscopic evidence that Tc(IV) replaces Fe(III) in an octahedral site in the magnetite structure.[55] Biogenically derived vivianite ($Fe^{2+}Fe^{2+}_2(PO_4)_2 \cdot 8H_2O$) and siderite ($FeCO_3$) take up less Tc compared to biogenically derived magnetite, and overall higher Tc was released in solution upon oxidation.[55, 60]

Zachara et al., 2007[11] investigated the abiotic reduction of Tc(VII) by dissolved Fe(II) in pH 6–8 solutions under strictly anoxic conditions using an oxygen trap ($<7.5\times10^{-9}$ bar O_2). Tc(VII) was reduced rapidly and completely to a precipitated Fe–Tc(IV) form when 11 μM Tc(VII) was reacted with 0.4 mM Fe(II) at pH 7.0 and 8.0, while no significant reduction was observed over 1 month at pH 6.0, demonstrating that the reduction kinetics are strongly pH dependent. The Fe–Tc(IV) solid phase so formed is poorly ordered and dominated by Fe(II)-containing ferrihydrite with minor magnetite. Tc(IV) exhibited homogeneous spatial distribution within the precipitates with estimated composition of the solids is $Fe_T/Tc(IV) \approx 6$. Spectra of the precipitate from X-ray Absorption Near-Edge Spectroscopy (XANES) analyses show that Tc is in the reduced form [Tc(IV)]. The molecular environment of Tc(IV) is consistent with an octahedral Tc(IV) dimer bound in bidentate edge-sharing mode to octahedral Fe(III) associated with surface or vacancy sites in ferrihydrite. The oxidation rate of sorbed Tc(IV) in the Fe–Tc precipitate is considerably slower than $Tc(IV)O_2 \cdot nH_2O(s)$.

Initial adsorption of Tc(IV) onto ferrihydrite also resulted in incorporation of Tc(IV) in the resulting magnetite phase at high pH (10.5-13.1).[59] Subsequent air oxidation of the magnetite particles for up to 152 days resulted in only limited remobilization of the incorporated Tc(IV). X-ray absorption spectroscopy data indicated that the Tc(IV) was predominantly incorporated into the magnetite octahedral site in all systems studied. On re-oxidation in air, the incorporated Tc(IV) was recalcitrant to oxidative dissolution with less than 40% remobilization to solution despite significant oxidation of the magnetite to maghemite/goethite and all solid associated Tc remained as Tc(IV).

Computational studies found that Tc(IV) doping into the octahedral Fe sites in magnetite is possible, but other Tc oxidation states, especially Tc(V), may be present and several mechanisms can balance the charge mismatch created when Tc(IV) replaces Fe(III) on the octahedral site.[61] To achieve Tc doping into Fe_3O_4, charge may be balanced by either replacement of Fe(III) by Fe(II) or by creating octahedral vacancies, however overall Tc(IV) incorporation into magnetite is energetically favorable.[61]

Overall mixed Fe(II)/Fe(III) precipitates of this nature may form in anoxic sediments or groundwater. The overall results of studies summarized in this section suggest that once Tc is immobilized as sorbed/precipitated Tc(IV) in Fe(II)/Fe(III) minerals, its remobilization upon the return of oxidizing conditions may be limited.

4.5.4. Tc coprecipitation process with Fe(II) containing sulfides and silicates

Livens et al.[57] showed that reduced Tc is harbored by mackinawite (tetragonal FeS) and EXAFS data indicates the presence of Tc-S bonds. During re-oxidation mackinawite

forms goethite [α-FeO(OH)], yet Tc remains in the reduced state. The EXAFS evidence indicates that Tc(IV) bonds switch from S to O suggesting that Tc(IV) may be incorporated into the goethite structure. Because of the identical size of the Tc(IV) and Fe(III) cations, this is a plausible substitution, provided that a charge-compensating ion is present or the solid forms a defect structure. These results were similar to those reported by Wharton et al.[58] in that FeS solids oxidized, but Tc remained reduced as was associated with O, rather than S, after re-oxidation. Tc incorporated into Fe(II)-bearing phyllosilicates along cracks or defect trails could also be reduced to Tc(IV), albeit more slowly than the mineral-surface mediated reduction mechanism.[12, 15, 62] Fe-bearing di- and trioctahedral phyllosilicates in various states of weathering are common in most sedimentary deposits and may be an important sink for reduced Tc. As reported by Fredrickson et al.[62] reduced Tc incorporated into diffusion- limited spaces, such as in phyllosilicates, is resistant to oxidation, whereas Tc(IV) on unprotected mineral surfaces rapidly re-oxidizes when contacted by air or oxidizing solutions.

4.5.5. Tc coprecipitation process with Fe(III) minerals

Lukens and Saslow[51] showed that coprecipitation of hematite (alpha-Fe_2O_3) with TcO_4^- in acidic conditions results in >80% Tc incorporation in the mineral structure, corresponding to a 2.2%wt uptake of Tc by the hematite structure. Leeching studies showed that that less <5% Tc are remobilized in 200 days of exposure to oxidative conditions. Incorporation of Tc into hematite has also been studied computationally, and up to 2.6 wt.% of isolated Tc(IV) can be accommodated by hematite when the charge is balanced by reduction of a neighboring Fe(III) site to Fe(II).[50] Although pertechnetate incorporation is found to be unfavorable, incorporation of small amounts of Tc(IV) (at least 2.6 wt. %) is energetically feasible.

Tc-doped goethite has been investigated both experimentally and computationally. [53, 54, 61] Um et al. 2011[53] demonstrated that Fe(II) sorbed to goethite efficiently catalyzes the reduction of Tc in deionized water and complex solutions that mimic the chemical composition of caustic waste scrubber media. Analyses of the Tc-bearing solid products by XAFS indicate that all of the Tc(VII) was reduced to Tc(IV) and that the latter is incorporated into goethite or magnetite as octahedral Tc(IV). Batch dissolution experiments, conducted under ambient oxidizing conditions for more than 180 days, demonstrated a very limited release of Tc to solution (27μg Tc/g solid). When crystals of goethite are furthered "armored" by an additional layer of precipitated goethite the armoring isolates the reduced ^{99}Tc(IV) from oxidizing agents. [54] Monolithic pellets formed from “armored” maintained Tc as a reduced species even after 120 days of oxidative leaching (pH = 7.2 and I = 0.05 M). The results of this study indicate that Tc can be immobilized in a stable, low-cost Fe oxide matrix that is easy to fabricate and these findings can be useful in designing long-term solutions for nuclear waste disposal.[54]

Collectively, these studies indicate that co-precipitation of Tc with an iron (oxy)hydroxide, sulfide, “green rust” or siderite provide a good medium of immobilization for Tc and remobilization upon oxidation is limited. Further, these studies

indicate that Tc incorporated into phyllosilicates is resistant to re-oxidation. The Tc(IV) in this case is associated with structural Fe and the resistance to re-oxidation appears to be subject to the limitation of oxygen diffusion into the phyllosilicates. These observations have implications for the designing a durable medium to immobilize Tc from liquid waste and additionally they provide insights into environmental and geological conditions that limit Tc mobility in the subsurface, which provide insight into canister corrosion impacts on Tc release and longterm contaminant mitigation.

5. Selenium interactions with Fe oxide minerals

5.1. Selenium

The trace element selenium (Se) is of special concern because of the extremely fine line between its opposing properties: at low concentrations, it is an essential nutrient for many organisms, at slightly higher quantities, however, it becomes a toxic contaminant.[63] Of concern are therefore not only Se-deficient agricultural soils in certain regions of the world, but also Se contaminations of soils or wastewaters caused by natural and/or anthropogenic factors. [63, 64]

In addition, selenium occurs in high-level nuclear waste (HLW) in the form of radionuclide ^{79}Se, which plays an important role in long-term safety assessments of deep geological repositories.[65] ^{79}Se is produced by nuclear fission and it is produced with a yield of about 0.04% [7] and is a component of spent nuclear fuel, high-level radioactive wastes resulting from processing spent fuel, and radioactive wastes associated with the operation of nuclear reactors and fuel reprocessing plants. The assumed concentration ^{79}Se in high-level radioactive waste is 10^{-7} mol/L and could amount to 10^{-10} mol/L in the biosphere.[66, 67]

^{79}Se is a pure beta-emitting nuclide, which poses a challenging task for reliable, quantitative determination of its half-life due to vulnerable radiometric and mass spectrometric methodologies, both requiring chemical purification in advance for the removal of interfering activity and isobars. The most recent measurements of ^{79}Se half-life report a value of $3.27(8)\times10^{5}$.[65] Due to its long half-life, it is one of only a few nuclides that determine the long-term radiological impact and of a repository on the environment.[68, 69]

5.2. Oxidation state

In nature selenium can occur in five different oxidation states (-II, -I, 0, IV, VI) and standard potential for redox reaction are reported in Table 5. Selenium species of the oxidation states Se(-II), Se(-I) and Se(0) are characterized by forming sparingly soluble compounds, including metal selenides or elemental Se.[66] By contrast in the two higher oxidations states, selenium forms the soluble oxyanions selenite [$Se^{IV}O_3^{2-}$] and selenate [$Se^{VI}O_4^{2-}$], which are generally highly mobile due to their limited interaction with geological materials.[66, 70, 71] In soils in contact with the atmosphere for example, the thermodynamically favored Se species are the oxyanions selenate [Se(VI)] and selenite

[Se(IV)]. The oxidation state is therefore the key factor determining the biogeochemical behavior of selenium, since parameters such as solubility, mobility, bioavailability and toxicity mainly depend on the occurrence of dissolved selenium species.[72, 73]

The selenium oxidation state in high level waste and the accompanying dominant selenium species depends on the waste type. Recent research has demonstrated that ^{79}Se occurs as Se(−II) in spent nuclear fuel.[74, 75] Due to the reducing conditions predicted in deep repositories, formation of mobile selenium species is unlikely, however, it cannot be fully excluded that oxidation processes induced by long-term irradiation could lead to a oxidation to Se(VI).[76] The fate of selenium in the near-field of high-level radioactive waste also depends on the Se valence state in vitrified glasses which are part of the technical barrier in the multibarrier concept for HLW disposal.[70] The expected predominant selenium oxidation state in vitrified HLW arising from nuclear fuel reprocessing plants is Se(IV) in the form of selenite.[76]

For these reasons it is imperative to understand the mobility of oxidized and reduced forms of Se in oxidizing and reducing conditions, to better determine long-term safety and performance of nuclear repository.

Table 5 Standard potential of Se redox reactions from Seby et al.[67]

Redox reactions	*Standard potential (V)*
Se(0)/Se(–II)	
$Se(s) + 2H^+ + 2e^- \Leftrightarrow H_2Se(aq)$	– 0.115
$Se(s) + H^+ + 2e^- \Leftrightarrow HSe^-$	– 0.227
$Se(s) + 2e^- \Leftrightarrow Se^{2-}$	– 0.641
Se(IV)/Se(0)	
$H_2SeO_3(aq) + 4H^+ + 4e^- \Leftrightarrow Se(s) + 3H_2O$	0.740
$HSeO_3^- + 5H^+ + 4e^- \Leftrightarrow Se(s) + 3H_2O$	0.780
$SeO_3^{2-} + 6H^+ + 4e^- \Leftrightarrow Se(s) + 3H_2O$	0.903
Se(VI)/Se(IV)	
$HSeO_4^- + 3H^+ + 2e^- \Leftrightarrow H_2SeO_3(aq) + H_2O$	1.090
$HSeO_4^- + 2H^+ + 2e^- \Leftrightarrow HSeO_3^- + H_2O$	1.008
$HSeO_4^- + H^+ + 2e^- \Leftrightarrow SeO_3^{2-} + H_2O$	0.760
$SeO_4^{2-} + 4H^+ + 2e^- \Leftrightarrow H_2SeO_3(aq) + H_2O$	1.139
$SeO_4^{2-} + 3H^+ + 2e^- \Leftrightarrow HSeO_3^- + H_2O$	1.060
$SeO_4^{2-} + 2H^+ + 2e^- \Leftrightarrow SeO_3^{2-} + H_2O$	0.811

5.3. Precipitation of Se compounds and their solubility

Selenium can react with inorganic cations to give solid phases that can be responsible for its immobilization. Precipitation/ dissolution reactions govern selenium solubility only in reduced conditions with formation of solid elemental selenium and metal-selenide((Se(-

2)).[77-80] Under reduced conditions, metal-selenide minerals are found to limit the Se solubility.[80] The most stable minerals are Cu_2Se(s) in acid soils and PbSe(s) and SnSe(s) under neutral to alkaline conditions.[80] In groundwater with a potential value lower than 0 mV, FeSe(s), ZnSe(s) and MnSe(s) can exist.[67] Equilibrium thermodynamic calculation have shown that elemental Se,FeSe(s) (achavalite) or $FeSe_2$(s) (ferroselite) can control Se solubility.[78, 81] Elemental Se has a wide stability field under acid conditions and formation of achavalite is favored for neutral to alkaline conditions. A mixed solid solution phase can also be formed with selenide substituting for sulfide and precipitated FeS will contain FeSe.[67] These observation of Se compounds solubility suggests that the chemistry of selenium is closely related to those of iron sulfides.[67]

Metal-selenate minerals are too soluble to persist in aerated soils and among different metal-selenite precipitates, only $MnSeO_3$(s) can be formed in strongly acid soils.[80]

5.4. Sorption processes: adsorption, surface mediated reduction and coprecipitation

5.4.1. Adsorption studies

The fate of dissolved Se(IV) and Se(VI) species in subsurface systems is primarily determined by interaction with mineral phases, including processes such as adsorption, incorporation, and reductive precipitation, which are the key immobilization mechanisms.[70, 82] However, most natural materials like clays or silicate minerals show only a restricted retention capacity for Se oxyanions.[83] In this context, crystalline iron (oxyhydr)oxide minerals (e.g. hematite and goethite) and their metastable precursors (e.g. ferrihydrite) are of great importance as they are widespread in nature and capable of anion sorption.[84, 85] This is the reason why, in particular, the mechanisms of Se oxyanion adsorption to iron oxide surfaces have been investigated in detail by a large number of previous studies.

Adsorption of Se(IV) and Se(VI) onto iron oxides can be very efficient at lower pH but is limited under near-neutral and alkaline pH conditions.[86-90] This tendency is independent of the type of iron oxide, since alkaline conditions generally lead to the formation of a negative charge at the iron oxide surface and therefore to a poor adsorption of anionic species.[71] Moreover, all iron oxides show a relatively high adsorption capacity for Se(IV) and there is only little release of Se(IV) with increasing ionic strength.

Unlike Se(IV), adsorption of Se(VI) is much lower and is strongly influenced by the presence of competing anions.[91-95] Most authors suggest the difference between Se(IV) and Se(VI) adsorption is due to the nature of the chemical attachment and the formation of different types of adsorption complexes.

Spectroscopic investigations as well as surface complexation modeling reveal that the adsorption of Se(IV) onto iron oxides is usually the result of inner-sphere complexation[71] with a mostly bidentate character, e.g. for hematite.[88, 96] By contrast, the poor adsorption of Se(VI) and the strong impact of competing anions has been attributed to the formation

of outer-sphere complexes.[91] However, more recent studies suggest that adsorption of Se(VI) can occur via both inner-sphere and outer-sphere complexation.[94, 97] The type of surface complexation depends on pH, ionic strength, the nature of the iron oxide mineral and its surface loading.[71, 98]

Several anions can be in competition with selenium ion sorption. Kim et al.[99] analyzed the influence of carbonate and silicate on the sorption of selenium ions onto magnetite. Se(IV) was sorbed onto magnetite very well below pH 10, but silicate and carbonate hindered its sorption onto magnetite. On the other hand, little Se(VI) was sorbed onto magnetite in neutral and weak alkaline solutions even though silicate or carbonate was not contained in the solutions. Seby et al.[67] report the following sequences for selenium sorption anion competitions on goethite: phosphate > silicate ~ citrate > molybdate > bicarbonate/carbonate > oxalate > fluoride > sulphate.[67]

Although a considerable amount of Se sorption data has been obtained under aerobic conditions, where selenite and selenate species are dominant, the data obtained under reducing conditions are limited and the sorption data for Se(-II) species are scarce. Iida et al.[100] performed batch sorption experiments of Se(-II) under reducing conditions to investigate the sorption behavior of selenium onto granodiorite, sandy mudstone, tuffaceous sandstone, and their major constituent minerals and accessory minerals (Table 6). The author conclude that minor phases present in granodiorite and sandstone, mainly biotite and pyrite, are important minerals with respect to the sorption behavior of Se onto rocks. Selected published K_d values for Se(-II), Se(V) and Se(VI) are reported in Table 6.

Table 6 Selected sorption K_d of Se onto geologic materials

Study	Se	Geologic material	Kd (as reported)
Borsig (2018)[101]	Se(VI)	magnetite (pH=9-9.3)	2.14-4.72 Log K_d (L/kg)
	Se(IV)	magnetite (pH=9-9.3)	4.7-5.16 Log K_d (L/kg)
Missana (2009)[83]	Se(IV)	smectite (pH 3-8)	500 mL/g (pH 3); 100 mL/g (pH 8)
		illite (pH 3-8)	150 mL/g (pH 3); 75 mL/g (pH8)1
Loyo(2008) [102]	Se(IV)	magnetite (pH 5)	3500-3600 mL/g
		magnetite (pH 10)	170 mL/g
		Fe/Fe_3C (pH 5)	3640-3800 mL/g
		Fe/Fe_3C (pH 10)	388-410 mL/g
Kim (2012) [99]	Se(IV)	magnetite (pH 7)	2000 mL/g
		magnetite pH 7 (10mmol/L carbonate-)	1300 mL/g
		magnetite (pH 9)	1200 mL/g
		magnetite (pH 9)	300 mL/g
	Se(VI)	magnetite a(6-8) (10mmol/L carbonate-)	no sorption
Fevrier (2007)[103]	Se(IV)	soil (sterile)	16 L/kg
		soil (non-sterile)	130 L/kg
Iida (2011) [100]	Se(-II)	granodiorite (pH 8.5-11.5)	$2.2x10^{-4}$ to 4 $x10^{-3}$ m^3/kg
	Se(-II)	sandy mudstone (pH 8.5-11.5)	$3.3x10^{-2}$ to $5.6x10^{-2}$ m^3/kg
	Se(-II)	tuffaceous sandstone (pH 8.5-11.5)	$2.9x10^{-2}$ to $8.2x10^{-2}$ m^3/kg

5.4.2. Surface mediated reduction of selenium

The oxidation state of dissolved selenium oxyanions can be reduced by Fe(II). Although the presence of dissolved Fe(II) generally favors the selenium reduction process,[104] a reduction only by dissolved Fe(II) is not possible due to the difference in reduction potentials of the redox couples.[105] It is known however that for the reduction by Fe(II) to occur, Se needs to interact with the surface of Fe(II) mineral[106] and various mineral phases that contain Fe(II) are able to reduce selenium oxyanions under anoxic conditions. This reduction process has been observed for magnetite[107] , iron(II) hydroxide[108, 109], green rust[110-112] as well as elemental iron,[113-116], iron(II) sulfides[107, 117] or Fe^{2+} adsorbed on clay minerals[118].

Since reduction of selenium oxyanions causes the formation of sparely soluble compounds, this interaction generally results in the immobilization of selenium. These selenium compounds are either elemental Se or iron selenides like FeSe and Fe_7Se_8, and the nature of the products varies depending on the iron-bearing phases, the hydrogeochemical conditions, and the reduction kinetics. Kinetic rather than thermo-dynamic control of reduction products may explain why the majority of the above-mentioned studies showed the formation of elemental Se(0)[106, 108-110, 112, 118, 119] and only a few studies identified iron selenides.[107, 113, 120] This can be attributed to the fact that

reduction to Se(-II) and formation of iron selenides is limited to a rapid reduction of selenium oxyanions.[107]

5.4.3. Coprecipitation studies

The coprecipitation and structural incorporation of a metal species in a mineral host can be relevant in cases where mineral phases interact with dissolved species during their formation or transformation, including recrystallization or sorption induced crystal growth. Since the formation pathway of crystalline iron oxides commonly includes amorphous metastable intermediates [121], such processes are very common in natural systems like soils. Oxyanion incorporation or occlusion by Fe(II) and Fe(II/III) minerals has been shown for Se(IV) [122], P(V)[123], As(V)[124, 125], and Tc(VII)[50]. For this reason, it is conceivable that a retention mechanism on the basis of incorporation also exists for the both Se oxyanions, Se(IV) and Se(VI), and that such mechanisms could affect the migration of dissolved Se species.

In reducing conditions, where reduced Se species are more stable, pyrite (FeS_2) and mackinawite (FeS) are expected to be the most dominant Fe(II) minerals. Pyrite is the most common near-surface iron sulfide, well-known for its capacity to incorporate elements up to several mol%.[126-129] Pyrite is also part of host rocks and bentonite backfills considered for use in HLW repositories[130-133] and could form from the corrosion of steel containers containing vitrified nuclear waste. Due to the similarities in geochemical behavior and ionic radii of Se(-II) and S(-II), iron sulfide minerals are likely host for selenide incorporation.

In the following sections we will discuss studies that have addressed the coprecipitation and structural incorporation of selenium in various Fe minerals, and a summary of the results is reported in Table 7.

Table 7 Summary of Se coprecipitation studies with Fe minerals (n.d.= not determined in study)

Study	Mineral	Se form	Se uptake (%)	Se behavior upon coprecipitation
Borsig et al 2018[101]	Magnetite (pH 9.2)	Se(IV) Se(VI)	100% 100% (10^{-4}-10^{-3} mol/L); 30% 10^{-2} mol/L	Reduction of Se(IV) or Se(VI) to Se(-II) causes the formation of nanoparticulate iron selenide [FeSe] phase. Progressive oxidation of Fe(II) hydroxide and green rust into magnetite leads to oxidation of Se(-II) to Se(0) (gray elemental selenium)
Missana et al. (2009) [134]	Magnetite (pH <5): adsorption studies at pH<5 showed magnetite dissolution and coprecipitation of Se species	Se(IV)	n.d.	Ferric selenite formation is the predominant retention process at higher selenite concentrations (>1 x10^{-4} M) and pH < 5
Diener 2011[135]	Pyrite, mackinawite (pH 4.5-5)	Se(-II)	98.9% (pyrite); 95.4% (mackinawite); 99.2% (amorphous FeS); 98.1% (mixed iron sulfide phases)	Focused ion beam analysis shows an inhomogeneous Se distribution with a higher accumulation in the center of the pyrite grains, probably due to the progressive depletion of Se from solution with regard to S.
Diener 2012[136]	Pyrite, mackinawite (pH 3.7-5)	Se(-II) Se(IV)	98.6 - 99.98 % 99.5%	In supersaturated solutions: substitution of S(-I) by Se(-I) in Se-doped pyrite and of S(-II) by Se(-II) in Se-doted mackinawite. At lower concentrations and in case of a slower precipitation : Se(-II) and Se(IV) retention by incorporation is coupled with a change in the oxidation state and selenium is incorporated as Se(0) into pyrite without structural bonding.
Francisco (2018)[137]	Ferrihydrite (pH 5-10)	Se(IV)	94-99% During aging, the behavior of Se(IV) varied with pH. At pH 5, Se was retained in the solid. At pH 10, a fraction of Se(IV) was released in solution.	Se(IV) was retained within the crystalline post-aging products and possibly occluded in nanopore and defect structures.
Borsig 2017 [138]	Ferrihydrite to hematite (pH 7.5)	Se(IV) Se(VI)	100% 15%	Se oxidation state is not changed during adsorption or coprecipitation. Se coprecipitation leads to the occurrence of a resistant, non-desorbable Se fraction. Se initially adsorbs to the ferrihydrite surface, but after the transformation of ferrihydrite into hematite, it is mostly incorporated by hematite.

5.4.4. Se coprecipitation process with Fe(II) and Fe(II)/Fe(III) oxy-hydroxides

Borsig et al.[101] investigated the immobilization of dissolved Se(IV) and Se(VI) during the formation of magnetite in coprecipitation experiments based on the progressive oxidation of an alkaline, anoxic Fe(II) system at pH 9.2. Results showed a high retention of selenium oxyanions during the mineral formation process. The authors show that this immobilization is due to the reduction of Se(IV) or Se(VI), resulting in the precipitation of sparingly soluble trigonal elemental selenium compounds. These selenium compounds formed in all coprecipitation products following magnetite formation. Time-resolved analysis of selenium speciation during magnetite formation and detailed spectroscopic analyses of the solid phases showed that selenium reduction occurred under anoxic conditions during the early phase of the coprecipitation process via interaction with Fe(II) hydroxide and green rust. This early selenium interaction leads to the formation of a nanoparticulate iron selenide phase [FeSe], which is oxidized and transformed into gray trigonal elemental selenium during the progressive oxidation of the aquatic system. Selenium is retained regardless of whether the oxidation of the unstable iron oxides leads to the formation of pure magnetite or other iron oxide phases, e.g. goethite.

Missana et al.[134] studied Se(IV) retention by magnetite using both surface complexation modeling and x-ray absorption spectroscopy (XAS) to characterize the processes of adsorption, reduction, and dissolution/co-precipitation. Results showed that at higher selenite concentrations ($>1\times10^{-4}$M) and pH<5 the precipitation of ferric selenite (SeIV-Fe) is the predominant retention process of Se onto magnetite.

5.4.5. Se coprecipitation process with sulfides

Selenium is often associated with sulfides such as pyrite, a frequent minor constituent of host rocks and bentonite backfills considered for radioactive waste disposal. Diener and Neumann[135] investigated the uptake of Se by pyrite (FeS_2) and mackinawite (FeS). More than 98% of the Se added to solutions was taken up by the Fe sulfide minerals. Focused ion beam analysis shows an inhomogeneous Se distribution with a higher accumulation in the center of the pyrite grains, probably due to the progressive depletion of Se from solution with regard to S. The results imply that pyrite and its precursor phase, mackinawite, are efficient in removing selenium from solution, and this may contribute in reducing the mobility of ^{79}Se released from radioactive waste.

Diener et al.[136] investigated the incorporation mechanisms of Se(-II) and Se(IV) into pyrite and mackinawite by x-ray absorption spectroscopy to determine the relevance of iron sulfides to Se retention and the type of structural bonding. The syntheses of pyrite and mackinawite occurred via direct precipitation in batches and also produced coatings on natural pyrite in mixed-flow reactor experiments under anoxic conditions at Se concentrations in the solutions of up to 10^{-3} mol/L. The Se uptake >98.6% suggesting a high potential for retention. XAFS results indicate a substitution of sulfur by selenide during instantaneous precipitation in highly supersaturated solutions only. In selenide

doped mackinawite, S(-II) was substituted by Se(-II), resulting in a mackinawite-type compound. S(-I) is substituted by Se(-I) in selenide-doped pyrite, yielding a FeSSe compound as a slightly distorted pyrite structure. Under slighter supersaturated conditions, XAFS results indicate an incorporation of S(-II) and Se(IV) predominantly as Se(0). This study shows that a substitution of S by Se in iron sulfides is probable only for highly supersaturated solutions under acidic and anoxic conditions, however under closer equilibrium conditions, Se(0) is expected to be the most stable species.

5.4.6. Se coprecipitation process with Fe(III) minerals

Francisco et al.[137] studied the coprecipitation behavior of Se(IV) with ferrihydrite at different pH values to determine how Se(IV) associates with ferrihydrite and how Se(IV) coordination changes with ferrihydrite aging and recrystallization. Results show that despite efficient removal, the mode and stability of Se(IV) retention in the coprecipitates varied with pH. At pH 5, Se(IV) is removed dominantly as a ferric selenite-like phase intimately associated with ferrihydrite, while at pH 10, it is mostly present as a surface species on ferrihydrite. Similarly, the behavior of Se(IV) and the extent of its retention during phase transformation varied with pH. At pH 5, Se(IV) remained completely associated with the solid phase despite recrystallization to hematite, whereas it was partially released back into solution at pH 10. Regardless of this difference in behavior, TEM and XAS results show that Se(IV) is retained within the crystalline products and possibly occluded in nanopore and defect structures. These results demonstrate a potential long-term immobilization pathway for Se(IV) even after phase transformation.

Borsig et al.[138] also studied the immobilization of Se oxyanions during the crystallization of hematite from ferrihydrite. In coprecipitation studies, hematite was synthesized by the precipitation and aging of ferrihydrite in an oxidized Se(IV) or Se(VI) containing system (pH 7.5). Aqueous chemistry data of these batch experiments revealed the complete uptake of all available Se(IV), while the retention of Se(VI) was low (max. 15% of Se). The study shows that during the crystallization of hematite from ferrihydrite, interacting Se oxyanions are not adsorbed but mainly incorporated into hematite. This incorporation process follows the previous adsorption of Se oxyanions onto ferrihydrite and takes place during the subsequent transformation of amorphous ferrihydrite into crystalline hematite. The incorporation mechanism itself results from a direct linkage between the Se oxyanions and the hematite phase but is not attributed to substitution or occupation of crystallographic sites within the hematite crystal lattice. The incorporated Se oxyanion species are bound to the hematite phase in a way that is similar to surface adsorption complexes – outer-sphere complexes for Se(VI) and innersphere complexes for Se(IV). Compared to simply adsorbed Se oxyanions, the retention of the incorporated Se fraction is very resistant even at alkaline pH conditions at least as long as the hematite mineral remains stable.

Collectively, these studies indicate that sorption processes of Se with Fe(III)(oxy)hydroxide, Fe(II) sulfide, and Fe(II/III) minerals provide a good medium of immobilization for Se. Key factors that affect removal of Se from solution include

mineral formation pathways, presence of Fe(II), pH and redox potential, and presence of competing anions.

Regarding the behavior of selenium in the geosphere, reductive selenium precipitation represents an efficient mechanism to immobilize dissolved selenium oxyanions. Processes like these should be considered in safety assessments of HLW disposal sites, as they may affect the migration of the radionuclide ^{79}Se as it interacts with secondary iron oxides in the near-field.

Although there is a significant body of literature discussing sorption processes of Se species with various reduced Fe minerals (Fe(II) and mixed Fe(II/FeIII)), there is a lack of information regarding the fate of Se species during re-oxidation and recrystallization reaction. Future studies should focus on determining the retention mechanisms of Se species after extended disposure to oxidative conditions, as has been done for Tc.

6. Future FY21 work

To mimic our ferrihydrite to goethite mineralization experiments, we are planning on performing magnetite experiments where Pu will be sorbed to a mineral precipitate precursor first, then aged to the desired mineral phase (green rust or magnetite). Our goal is to understand if differences in association of Pu to the precursor material will affect bonding of Pu to the final crystalline solid. In the magnetite synthesis a Fe-precipitate forms starting at pH>3. Our plan is to add Pu to the $Fe(III)Cl_3$ once the pH> 3 precipitate has formed. Then we will proceed with the synthesis as described above.
We also plan on expanding our literature review of radionuclides relevant to nuclear waste repository (i.e. Np, I and Cl) performance assessment, perform additional corrosion experiments for radionuclides with limited information in the literature (e.g. iodine), and evaluate the overall impact that nuclear waste repository corrosion processes on radionuclide release and long-term performance of nuclear waste repositories.

7. Acknowledgments

This work was supported by the Spent Fuel and Waste Science and Technology campaign of the Department of Energy's Nuclear Energy Program. Prepared by LLNL under Contract DE-AC52-07NA27344.

8. References

1. Kirsch, R.; Fellhauer, D.; Altmaier, M.; Neck, V.; Rossberg, A.; Fanghanel, T.; Charlet, L.; Scheinost, A. C., Oxidation state and local structure of plutonium reacted with magnetite, mackinawite, and chukanovite. *Environmental Science & Technology* **2011,** *45*, (17), 7267-7274.
2. Icenhower, J. P.; Qafoku, N. P.; Zachara, J. M.; Martin, W. J., THE BIOGEOCHEMISTRY OF TECHNETIUM: A REVIEW OF THE BEHAVIOR OF AN ARTIFICIAL ELEMENT IN THE NATURAL ENVIRONMENT. *American Journal of Science* **2010,** *310*, (8), 721-752.

3. Pilkington, N. J., The solubility of technetium in the near-field environment of a radioactive waste repository. *Journal of the Less Common Metals* **1990,** *161*, (2), 203-212.
4. Kunze, S.; Neck, V.; Gompper, K.; Fanghänel, T., Studies on the Immobilization of Technetium under Near Field Geochemical Conditions. *Radiochimica Acta* **1996,** *74*, (Supplement), 159-164.
5. Schulte, E. H.; Scoppa, P., SOURCES AND BEHAVIOR OF TECHNETIUM IN THE ENVIRONMENT. *Science of the Total Environment* **1987,** *64*, (1-2), 163-179.
6. Darab, J. G.; Smith, P. A., Chemistry of technetium and rhenium species during low-level radioactive waste vitrification. *Chemistry of Materials* **1996,** *8*, (5), 1004-1021.
7. Meyer, R. E.; Arnold, W. D.; Case, F. I.; Okelley, G. D., Solubilities of Tc(Iv) Oxides. *Radiochimica Acta* **1991,** *55*, (1), 11-18.
8. Boyd, G. E., Osmotic and Activity-Coefficients of Aqueous Natco4 and Nareo4 Solutions at 25-Degrees-C. *Journal of Solution Chemistry* **1978,** *7*, (4), 229-238.
9. EPA EPA facts about Technetium-99. https://semspub.epa.gov/work/HQ/175252.pdf
10. Cui, D. Q.; Eriksen, T. E., Reduction of pertechnetate by ferrous iron in solution: Influence of sorbed and precipitated Fe(II). *Environmental Science & Technology* **1996,** *30*, (7), 2259-2262.
11. Zachara, J. M.; Heald, S. M.; Jeon, B. H.; Kukkadapu, R. K.; Liu, C. X.; McKinley, J. P.; Dohnalkova, A. C.; Moore, D. A., Reduction of pertechnetate Tc(VII) by aqueous Fe(II) and the nature of solid phase redox products. *Geochimica Et Cosmochimica Acta* **2007,** *71*, (9), 2137-2157.
12. Peretyazhko, T.; Zachara, J. M.; Heald, S. M.; Jeon, B. H.; Kukkadapu, R. K.; Liu, C.; Moore, D.; Resch, C. T., Heterogeneous reduction of Tc(VII) by Fe(II) at the solid-water interface. *Geochimica Et Cosmochimica Acta* **2008,** *72*, (6), 1521-1539.
13. Peretyazhko, T.; Zachara, J. M.; Heald, S. M.; Kukkadapu, R. K.; Liu, C.; Plymale, A. E.; Resch, C. T., Reduction of Tc(VII) by Fe(II) sorbed on Al (hydr)oxides. *Environmental Science & Technology* **2008,** *42*, (15), 5499-5506.
14. Colton, R., Chemistry of Rhenium and Technetium. *Journal of the Less-Common Metals* **1966,** *11*, (2), 147-&.
15. Fredrickson, J. K.; Zachara, J. M.; Balkwill, D. L.; Kennedy, D.; Li, S. M. W.; Kostandarithes, H. M.; Daly, M. J.; Romine, M. F.; Brockman, F. J., Geomicrobiology of high-level nuclear waste-contaminated vadose sediments at the Hanford Site, Washington State. *Applied and Environmental Microbiology* **2004,** *70*, (7), 4230-4241.
16. Krebs, B.; Hasse, K.-D., Refinements of the crystal structures of KTcO4, KReO4 and OsO4. The bond lengths in tetrahedral oxoanions and oxides of d0 transition metals. *Acta Crystallographica Section B* **1976,** *32*, (5), 1334-1337.
17. Bandoli, G.; Mazzi, U.; Roncari, E.; Deutsch, E., Crystal structures of technetium compounds. *Coordination Chemistry Reviews* **1982,** *44*, (2), 191-227.
18. Baston, G. M. N.; De Canniere, P. R.; Ilett, D. J.; Cowper, M. M.; Pilkington, N. J.; Tweed, C. J.; Wang, L.; Williams, S. J., Technetium behaviour in Boom Clay - a laboratory and field study. *Radiochimica Acta* **2002,** *90*, (9-11), 735-740.
19. Farrell, J.; Bostick, W. D.; Jarabek, R. J.; Fiedor, J. N., Electrosorption and reduction of pertechnetate by anodically polarized magnetite. *Environmental Science & Technology* **1999,** *33*, (8), 1244-1249.
20. Eriksen, T. E.; Ndalamba, P.; Bruno, J.; Caceci, M., The Solubility of TcO2 · nH2O in Neutral to Alkaline Solutions under Constant pco2. **1992,** *58-59*, (1), 67.
21. Meyer, R. E.; Arnold, W. D.; Case, F. I. *The solubility of electrodeposited Tc(IV) oxides*; NUREG/CR-4865; ORNL-6374; Other: ON: DE87013034 United States Other: ON: DE87013034 NTIS, PC A02/MF A01 - GPO. HEDB English; ; Oak Ridge National Lab.,

TN (USA); Nuclear Regulatory Commission, Washington, DC (USA). Office of Nuclear Regulatory Research: 1987; p Medium: X; Size: Pages: 20.
22. Warwick, P.; Aldridge, S.; Evans, N.; Vines, S., The solubility of technetium(IV) at high pH. *Radiochimica Acta* **2007,** *95*, (12), 709-716.
23. Liu, D. J.; Yao, J.; Wang, B.; Bruggeman, C.; Maes, N., Solubility study of Tc(IV) in a granitic water. *Radiochimica Acta* **2007,** *95*, (9), 523-528.
24. Langmuir, D., *Aqueous Environemntal Geochemistry*. Upper Saddle River, New Jersey, Prentice Hall: 1997.
25. Hess, N. J.; Xia, Y.; Rai, D.; Conradson, S. D., Thermodynamic Model for the Solubility of TcO2· xH2O(am) in the Aqueous Tc(IV) – Na+ – Cl− – H+ – OH− – H2O System. *Journal of Solution Chemistry* **2004,** *33*, (2), 199-226.
26. Lieser, K. H.; Bauscher, C., Technetium in the Hydrosphere and in the Geosphere .1. Chemistry of Technetium and Iron in Natural-Waters and Influence of the Redox Potential on the Sorption of Technetium. *Radiochimica Acta* **1987,** *42*, (4), 205-213.
27. Boggs, M. A.; Minton, T.; Dong, W. M.; Lomasney, S.; Islam, M. R.; Gu, B. H.; Wall, N. A., Interactions of Tc(IV) with Humic Substances. *Environmental Science & Technology* **2011,** *45*, (7), 2718-2724.
28. Gu, B. H.; Dong, W. M.; Liang, L. Y.; Wall, N. A., Dissolution of Technetium(IV) Oxide by Natural and Synthetic Organic Ligands under both Reducing and Oxidizing Conditions. *Environmental Science & Technology* **2011,** *45*, (11), 4771-4777.
29. Maes, A.; Geraedts, K.; Bruggeman, C.; Vancluysen, J.; Rossberg, A.; Hennig, C., Evidence for the interaction of technetium colloids with humic substances by X-ray absorption spectroscopy. *Environmental Science & Technology* **2004,** *38*, (7), 2044-2051.
30. Vichot, L.; Ouvrard, G.; Montavon, G.; Fattahi, M.; Musikas, C.; Grambow, B., XAS study of technetium(IV) polymer formation in mixed sulphate/chloride media. *Radiochimica Acta* **2002,** *90*, (9-11), 575-579.
31. Sekine, T.; Narushima, H.; Suzuki, T.; Takayama, T.; Kudo, H.; Lin, A.; Katsumura, Y., Technetium(IV) oxide colloids produced by radiolytic reactions in aqueous pertechnetate solution. *Colloids and Surfaces a-Physicochemical and Engineering Aspects* **2004,** *249*, (1-3), 105-109.
32. Sekine, T.; Narushima, H.; Kino, Y.; Kudo, H.; Lin, M. Z.; Katsumura, Y., Radiolytic formation of Tc(IV) oxide colloids. *Radiochimica Acta* **2002,** *90*, (9-11), 611-616.
33. Pepper, S. E.; Bunker, D. J.; Bryan, N. D.; Livens, F. R.; Charnock, J. M.; Pattrick, R. A. D.; Collison, D., Treatment of radioactive wastes: An X-ray absorption spectroscopy study of the reaction of technetium with green rust. *Journal of Colloid and Interface Science* **2003,** *268*, (2), 408-412.
34. Kobayashi, T.; Scheinost, A. C.; Fellhauer, D.; Gaona, X.; Altmaier, M., Redox behavior of Tc(VII)/Tc(IV) under various reducing conditions in 0.1 M NaCl solutions. **2013,** *101*, (5), 323.
35. Hebel, L. C.; Christensen, E. L.; Donath, F. A.; Falconer, W. E.; Lidofsky, L. J.; Moniz, E. J.; Moss, T. H.; Pigford, R. L.; Pigford, T. H.; Rochlin, G. I.; Silsbee, R. H.; Wrenn, M. E.; Committee, A. P. S. C. R.; Frauenfelder, H.; Cairns, T. L.; Panofsky, W. K. H.; Simmons, M. G., Report to the American Physical Society by the study group on nuclear fuel cycles and waste management. *Reviews of Modern Physics* **1978,** *50*, (1), S1-S176.
36. DOE DOE's License Application for a High-Level Waste Geologic Repository at Yucca Mountain. https://www.nrc.gov/waste/hlw-disposal/yucca-lic-app.html
37. Mann, F. M. *Integrated Disposal Facility Risk Assessment*; United States, 2003; p 162.
38. SRR Closure & Waste Disposal Authority Aiken, S. *PERFORMANCE ASSESSMENT for the SALTSTONE DISPOSAL FACILITY at the SAVANNAH RIVER SITE*; SRR Closure & Waste Disposal Authority Aiken, SC 29808: Aiken, SC 29808, 2009.

39. Li, D.; Kaplan, D. I., Sorption coefficients and molecular mechanisms of Pu, U, Np, Am and Tc to Fe (hydr)oxides: A review. *Journal of Hazardous Materials* **2012,** *243*, 1-18.
40. Vandergraaf, T. T.; Ticknor, K. V.; George, I. M., Reactions Between Technetium in Solution and Iron-Containing Minerals Under Oxic and Anoxic Conditions. In *Geochemical Behavior of Disposed Radioactive Waste*, American Chemical Society: 1984; Vol. 246, pp 25-43.
41. Palmer, D. A.; Meyer, R. E., Adsorption of technetium on selected inorganic ion-exchange materials and on a range of naturally occurring minerals under oxic conditions. *Journal of Inorganic and Nuclear Chemistry* **1981,** *43*, (11), 2979-2984.
42. Kaplan, D., Influence of surface charge of an Fe-oxide and an organic matter dominated soil on iodide and pertechnetate sorption. *Radiochim Acta* **2002,** *91*, 173-178.
43. Sheppard, M. I.; Sheppard, S. C., Technetium Behaviour in Soils of the Canadian Precambrian Shield. In *Technetium in the Environment*, Desmet, G.; Myttenaere, C., Eds. Springer Netherlands: Dordrecht, 1986; pp 131-141.
44. Elwear, S.; German, K. E.; Peretrukhin, V. F., Sorption of Technetium on Inorganic Sorbents and Natural Minerals. *Journal of Radioanalytical and Nuclear Chemistry-Articles* **1992,** *157*, (1), 3-14.
45. Kaplan, D. I.; Serne, R. J., Pertechnetate Exclusion from Sediments. **1998,** *81*, (2), 117.
46. Muller, O.; White, W. B.; Roy, R., Crystal chemistry of some technetium-containing oxides. *Journal of Inorganic and Nuclear Chemistry* **1964,** *26*, (12), 2075-2086.
47. Ramanaidou, E.; Nahon, D.; Decarreau, A.; Melfi, A. J., Hematite and goethite from duricrusts developed by lateritic chemical weathering of Precambrian banded iron formations, Minas Gerais, Brazil. *Clays and Clay Minerals* **1996,** *44*, (1), 22-31.
48. Shuster, D. L.; Vasconcelos, P. M.; Heim, J. A.; Farley, K. A., Weathering geochronology by (U-Th)/He dating of goethite. *Geochimica et Cosmochimica Acta* **2005,** *69*, (3), 659-673.
49. Yapp, C. J., Climatic implications of surface domains in arrays of δD and δ18O from hydroxyl minerals: goethite as an example. *Geochimica et Cosmochimica Acta* **2000,** *64*, (12), 2009-2025.
50. Skomurski, F. N.; Rosso, K. M.; Krupka, K. M.; McGrail, B. P., Technetium Incorporation into Hematite (alpha-Fe2O3). *Environmental Science & Technology* **2010,** *44*, (15), 5855-5861.
51. Lukens, W. W.; Saslow, S. A., Facile incorporation of technetium into magnetite, magnesioferrite, and hematite by formation of ferrous nitrate in situ: precursors to iron oxide nuclear waste forms. *Dalton Transactions* **2018,** *47*, (30), 10229-10239.
52. Saslow, S. A.; Um, W.; Pearce, C. I.; Engelhard, M. H.; Bowden, M. E.; Lukens, W.; Leavy, I. I.; Riley, B. J.; Kim, D.-S.; Schweiger, M. J.; Kruger, A. A., Reduction and Simultaneous Removal of 99Tc and Cr by Fe(OH)2(s) Mineral Transformation. *Environmental Science & Technology* **2017,** *51*, (15), 8635-8642.
53. Um, W.; Chang, H. S.; Icenhower, J. P.; Lukens, W. W.; Serne, R. J.; Qafoku, N. P.; Westsik, J. H.; Buck, E. C.; Smith, S. C., Immobilization of 99-Technetium (VII) by Fe(II)-Goethite and Limited Reoxidation. *Environmental Science & Technology* **2011,** *45*, (11), 4904-4913.
54. Um, W.; Chang, H.; Icenhower, J. P.; Lukens, W. W.; Serne, R. J.; Qafoku, N.; Kukkadapu, R. K.; Westsik, J. H., Iron oxide waste form for stabilizing (TC)-T-99. *Journal of Nuclear Materials* **2012,** *429*, (1-3), 201-209.
55. McBeth, J.; Lloyd, J.; Law, G.; R. Livens, F.; T. Burke, I.; Morris, K., *Redox interactions of technetium with iron-bearing minerals*. 2011; Vol. 75, p 2419-2430.
56. Yalçıntaş, E.; Scheinost, A. C.; Gaona, X.; Altmaier, M., Systematic XAS study on the reduction and uptake of Tc by magnetite and mackinawite. *Dalton Transactions* **2016,** *45*, (44), 17874-17885.

57. Livens, F. R.; Jones, M. J.; Hynes, A. J.; Charnock, J. M.; Mosselmans, J. F. W.; Hennig, C.; Steele, H.; Collison, D.; Vaughan, D. J.; Pattrick, R. A. D.; Reed, W. A.; Moyes, L. N., X-ray absorption spectroscopy studies of reactions of technetium, uranium and neptunium with mackinawite. *Journal of Environmental Radioactivity* **2004,** *74*, (1-3), 211-219.
58. Wharton, M. J.; Atkins, B.; Charnock, J. M.; Livens, F. R.; Pattrick, R. A. D.; Collison, D., An X-ray absorption spectroscopy study of the coprecipitation of Tc and Re with mackinawite (FeS). *Applied Geochemistry* **2000,** *15*, (3), 347-354.
59. Marshall, T. A.; Morris, K.; Law, G. T. W.; Mosselmans, J. F. W.; Bots, P.; Parry, S. A.; Shaw, S., Incorporation and Retention of 99-Tc(IV) in Magnetite under High pH Conditions. *Environmental Science & Technology* **2014,** *48*, (20), 11853-11862.
60. Thorpe, C. L.; Boothman, C.; Lloyd, J. R.; Law, G. T. W.; Bryan, N. D.; Atherton, N.; Livens, F. R.; Morris, K., The interactions of strontium and technetium with Fe(II) bearing biominerals: Implications for bioremediation of radioactively contaminated land. *Applied Geochemistry* **2014,** *40*, 135-143.
61. Smith, F. N.; Um, W.; Taylor, C. D.; Kim, D.-S.; Schweiger, M. J.; Kruger, A. A., Computational Investigation of Technetium(IV) Incorporation into Inverse Spinels: Magnetite (Fe3O4) and Trevorite (NiFe2O4). *Environmental Science & Technology* **2016,** *50*, (10), 5216-5224.
62. Fredrickson, J. K.; Zachara, J. M.; Plymale, A. E.; Heald, S. M.; McKinley, J. P.; Kennedy, D. W.; Liu, C. X.; Nachimuthu, P., Oxidative dissolution potential of biogenic and abiogenic TcO2 in subsurface sediments. *Geochimica Et Cosmochimica Acta* **2009,** *73*, (8), 2299-2313.
63. Lenz, M.; Lens, P. N. L., The essential toxin: The changing perception of selenium in environmental sciences. *Science of The Total Environment* **2009,** *407*, (12), 3620-3633.
64. Winkel, L. H. E.; Johnson, C. A.; Lenz, M.; Grundl, T.; Leupin, O. X.; Amini, M.; Charlet, L., Environmental Selenium Research: From Microscopic Processes to Global Understanding. *Environmental Science & Technology* **2012,** *46*, (2), 571-579.
65. Jörg, G.; Bühnemann, R.; Hollas, S.; Kivel, N.; Kossert, K.; Van Winckel, S.; Gostomski, C. L. v., Preparation of radiochemically pure 79Se and highly precise determination of its half-life. *Applied Radiation and Isotopes* **2010,** *68*, (12), 2339-2351.
66. Séby, F.; Potin-Gautier, M.; Giffaut, E.; Borge, G.; Donard, O. F. X., A critical review of thermodynamic data for selenium species at 25°C. *Chemical Geology* **2001,** *171*, (3), 173-194.
67. Seby, F.; Potin-Gautier, M.; Giffaut, E.; Donard, O. F. X., Assessing the speciation and the biogeochemical processes affecting the mobility of selenium from a geological repository of radioactive wastes to the biosphere. *Analusis* **1998,** *26*, (5), 193-198.
68. Olyslaegers, G.; Zeevaert, T.; Pinedo, P.; Simon, I.; Prohl, G.; Kowe, R.; Chen, Q.; Mobbs, S.; Bergstrom, U.; Hallberg, B.; Katona, T.; Eged, K.; Kanyar, B., A comparative radiological assessment of five European biosphere systems in the context of potential contamination of well water from the hypothetical disposal of radioactive waste. *Journal of Radiological Protection* **2005,** *25*, (4), 375-391.
69. Barescut, J. C.; Gariel, J. C.; Péres, J. M.; Février, L.; Martin-Garin, A., Biogeochemical behaviour of anionic radionuclides in soil: Evidence for biotic interactions. *Radioprotection* **2005,** *40*, (S1), S79-S86.
70. Grambow, B., Mobile fission and activation products in nuclear waste disposal. *Journal of Contaminant Hydrology* **2008,** *102*, (3), 180-186.
71. Fernández-Martínez, A.; Charlet, L., Selenium environmental cycling and bioavailability: a structural chemist point of view. *Reviews in Environmental Science and Bio/Technology* **2009,** *8*, (1), 81-110.

72. Winkel, L. H. E.; Vriens, B.; Jones, G. D.; Schneider, L. S.; Pilon-Smits, E.; Banuelos, G. S., Selenium Cycling Across Soil-Plant-Atmosphere Interfaces: A Critical Review. *Nutrients* **2015,** *7*, (6), 4199-4239.
73. Nothstein, A. K.; Eiche, E.; Riemann, M.; Nick, P.; Winkel, L. H. E.; Gottlicher, J.; Steininger, R.; Brendel, R.; von Brasch, M.; Konrad, G.; Neumann, T., Tracking Se Assimilation and Speciation through the Rice Plant - Nutrient Competition, Toxicity and Distribution. *Plos One* **2016,** *11*, (4).
74. Curti, E.; Puranen, A.; Grolimund, D.; Jädernas, D.; Sheptyakov, D.; Mesbah, A., Characterization of selenium in UO2 spent nuclear fuel by micro X-ray absorption spectroscopy and its thermodynamic stability. *Environmental Science: Processes & Impacts* **2015,** *17*, (10), 1760-1768.
75. Curti, E.; Froideval-Zumbiehl, A.; Günther-Leopold, I.; Martin, M.; Bullemer, A.; Linder, H.; Borca, C. N.; Grolimund, D., Selenium redox speciation and coordination in high-burnup UO2 fuel: Consequences for the release of 79Se in a deep underground repository. *Journal of Nuclear Materials* **2014,** *453*, (1), 98-106.
76. Bingham, P. A.; Connelly, A. J.; Cassingham, N. J.; Hyatt, N. C., Oxidation state and local environment of selenium in alkali borosilicate glasses for radioactive waste immobilisation. *Journal of Non-Crystalline Solids* **2011,** *357*, (14), 2726-2734.
77. Masscheleyn, P. H.; Patrick, W. H., Biogeochemical Processes Affecting Selenium Cycling in Wetlands. *Environmental Toxicology and Chemistry* **1993,** *12*, (12), 2235-2243.
78. Masscheleyn, P. H.; Delaune, R. D.; Patrick, W. H., Biogeochemical Behavior of Selenium in Anoxic Soils and Sediments - an Equilibrium Thermodynamics Approach. *Journal of Environmental Science and Health Part a-Environmental Science and Engineering & Toxic and Hazardous Substance Control* **1991,** *26*, (4), 555-573.
79. Masscheleyn, P. H.; Delaune, R. D.; Patrick, W. H., Transformations of Selenium as Affected by Sediment Oxidation Reduction Potential and Ph. *Environmental Science & Technology* **1990,** *24*, (1), 91-96.
80. Elrashidi, M. A.; Adriano, D. C.; Workman, S. M.; Lindsay, W. L., Chemical-Equilibria of Selenium in Soils - a Theoretical Development. *Soil Science* **1987,** *144*, (2), 141-152.
81. Hatten Howard, J., Geochemistry of selenium: formation of ferroselite and selenium behavior in the vicinity of oxidizing sulfide and uranium deposits. *Geochimica et Cosmochimica Acta* **1977,** *41*, (11), 1665-1678.
82. Chen, F. R.; Burns, P. C.; Ewing, R. C., Se-79: geochemical and crystallo-chemical retardation mechanisms. *Journal of Nuclear Materials* **1999,** *275*, (1), 81-94.
83. Missana, T.; Alonso, U.; Garcia-Gutierrez, M., Experimental study and modelling of selenite sorption onto illite and smectite clays. *Journal of Colloid and Interface Science* **2009,** *334*, (2), 132-138.
84. Roh, Y.; Lee, S. Y.; Elless, M. P., Characterization of corrosion products in the permeable reactive barriers. *Environmental Geology* **2000,** *40*, (1-2), 184-194.
85. Adegoke, H. I.; Adekola, F. A.; Fatoki, O. S.; Ximba, B. J., Sorptive Interaction of Oxyanions with Iron Oxides: A Review. *Polish Journal of Environmental Studies* **2013,** *22*, (1), 7-24.
86. Balistrieri, L. S.; Chao, T. T., Adsorption of Selenium by Amorphous Iron Oxyhydroxide and Manganese-Dioxide. *Geochimica Et Cosmochimica Acta* **1990,** *54*, (3), 739-751.
87. Zhang, P. C.; Sparks, D. L., Kinetics of Selenate and Selenite Adsorption Desorption at the Goethite Water Interface. *Environmental Science & Technology* **1990,** *24*, (12), 1848-1856.
88. Duc, M.; Lefevre, G.; Fedoroff, M.; Jeanjean, J.; Rouchaud, J. C.; Monteil-Rivera, F.; Dumonceau, J.; Milonjic, S., Sorption of selenium anionic species on apatites and iron

oxides from aqueous solutions. *Journal of Environmental Radioactivity* **2003,** *70*, (1-2), 61-72.
89. Martínez, M.; Giménez, J.; de Pablo, J.; Rovira, M.; Duro, L., Sorption of selenium(IV) and selenium(VI) onto magnetite. *Applied Surface Science* **2006,** *252*, (10), 3767-3773.
90. Rovira, M.; Giménez, J.; Martínez, M.; Martínez-Lladó, X.; de Pablo, J.; Martí, V.; Duro, L., Sorption of selenium(IV) and selenium(VI) onto natural iron oxides: Goethite and hematite. *Journal of Hazardous Materials* **2008,** *150*, (2), 279-284.
91. Hayes, K. F.; Roe, A. L.; Brown Jr, G. E.; Hodgson, K. O.; Leckie, J. O.; Parks, G. A., In situ x-ray absorption study of surface complexes: Selenium oxyanions on α-FeOOH. *Science* **1987,** *238*, (4828), 783-786.
92. Su, C. M.; Suarez, D. L., Selenate and selenite sorption on iron oxides: An infrared and electrophoretic study. *Soil Science Society of America Journal* **2000,** *64*, (1), 101-111.
93. Rietra, R. P. J. J.; Hiemstra, T.; van Riemsdijk, W. H., Comparison of selenate and sulfate adsorption on goethite. *Journal of Colloid and Interface Science* **2001,** *240*, (2), 384-390.
94. Jordan, N.; Ritter, A.; Foerstendorf, H.; Scheinost, A. C.; Weiss, S.; Heim, K.; Grenzer, J.; Mucklich, A.; Reuther, H., Adsorption mechanism of selenium(VI) onto maghemite. *Geochimica Et Cosmochimica Acta* **2013,** *103*, 63-75.
95. Jordan, N.; Ritter, A.; Scheinost, A. C.; Weiss, S.; Schild, D.; Hubner, R., Selenium(IV) Uptake by Maghemite (gamma-Fe2O3). *Environmental Science & Technology* **2014,** *48*, (3), 1665-1674.
96. Catalano, J. G.; Zhang, Z.; Fenter, P.; Bedzyk, M. J., Inner-sphere adsorption geometry of Se(IV) at the hematite (100)-water interface. *Journal of Colloid and Interface Science* **2006,** *297*, (2), 665-671.
97. Wijnja, H.; Schulthess, C. P., Vibrational spectroscopy study of selenate and sulfate adsorption mechanisms on Fe and Al (hydr)oxide surfaces. *Journal of Colloid and Interface Science* **2000,** *229*, (1), 286-297.
98. Fukushi, K.; Sverjensky, D. A., A surface complexation model for sulfate and selenate on iron oxides consistent with spectroscopic and theoretical molecular evidence. *Geochimica Et Cosmochimica Acta* **2007,** *71*, (1), 1-24.
99. Kim, S. S.; Min, J. H.; Lee, J. K.; Baik, M. H.; Choi, J. W.; Shin, H. S., Effects of pH and anions on the sorption of selenium ions onto magnetite. *Journal of Environmental Radioactivity* **2012,** *104*, 1-6.
100. Iida, Y.; Tanaka, T.; Yamaguchi, T.; Nakayama, S., Sorption Behavior of Selenium(-II) on Rocks under Reducing Conditions. *Journal of Nuclear Science and Technology* **2011,** *48*, (2), 279-291.
101. Borsig, N.; Scheinost, A. C.; Shaw, S.; Schild, D.; Neumann, T., Retention and multiphase transformation of selenium oxyanions during the formation of magnetite via iron(II) hydroxide and green rust. *Dalton Transactions* **2018,** *47*, (32), 11002-11015.
102. López de Arroyabe Loyo, R.; Nikitenko, S. I.; Scheinost, A. C.; Simonoff, M., Immobilization of Selenite on Fe3O4 and Fe/Fe3C Ultrasmall Particles. *Environmental Science & Technology* **2008,** *42*, (7), 2451-2456.
103. Fevrier, L.; Martin-Garin, A.; Leclerc, E., Variation of the distribution coefficient (K-d) of selenium in soils under various microbial states. *Journal of Environmental Radioactivity* **2007,** *97*, (2-3), 189-205.
104. Tang, C.; Huang, Y. H.; Zeng, H.; Zhang, Z., Reductive removal of selenate by zero-valent iron: The roles of aqueous Fe2+ and corrosion products, and selenate removal mechanisms. *Water Research* **2014,** *67*, 166-174.
105. Chakraborty, S.; Bardelli, F.; Charlet, L., Reactivities of Fe(II) on Calcite: Selenium Reduction. *Environmental Science & Technology* **2010,** *44*, (4), 1288-1294.

106. Chen, Y.-W.; Truong, H.-Y. T.; Belzile, N., Abiotic formation of elemental selenium and role of iron oxide surfaces. *Chemosphere* **2009,** *74*, (8), 1079-1084.
107. Scheinost, A. C.; Kirsch, R.; Banerjee, D.; Fernandez-Martinez, A.; Zaenker, H.; Funke, H.; Charlet, L., X-ray absorption and photoelectron spectroscopy investigation of selenite reduction by FeII-bearing minerals. *Journal of Contaminant Hydrology* **2008,** *102*, (3), 228-245.
108. Murphy, A. P., Removal of selenate from water by chemical reduction. *Industrial & Engineering Chemistry Research* **1988,** *27*, (1), 187-191.
109. Zingaro, R. A.; Carl Dufner, D.; Murphy, A. P.; Moody, C. D., Reduction of oxoselenium anions by iron(II) hydroxide. *Environment International* **1997,** *23*, (3), 299-304.
110. Myneni, S. C. B.; Tokunaga, T. K.; Brown, G. E., Abiotic Selenium Redox Transformations in the Presence of Fe(II,III) Oxides. *Science* **1997,** *278*, (5340), 1106-1109.
111. Johnson, T. M.; Bullen, T. D., Selenium isotope fractionation during reduction by Fe(II)-Fe(III) hydroxide-sulfate (green rust). *Geochimica et Cosmochimica Acta* **2003,** *67*, (3), 413-419.
112. Scheidegger, A. M.; Grolimund, D.; Cui, D.; Devoy, J.; Spahiu, K.; Wersin, P.; Bonhoure, I.; Janousch, M., Reduction of selenite on iron surfaces: A micro-spectroscopic study. *Journal De Physique Iv* **2003,** *104*, 417-420.
113. Olegario, J. T.; Yee, N.; Miller, M.; Sczepaniak, J.; Manning, B., Reduction of Se(VI) to Se(-II) by zerovalent iron nanoparticle suspensions. *Journal of Nanoparticle Research* **2010,** *12*, (6), 2057-2068.
114. Yoon, I.-H.; Kim, K.-W.; Bang, S.; Kim, M. G., Reduction and adsorption mechanisms of selenate by zero-valent iron and related iron corrosion. *Applied Catalysis B: Environmental* **2011,** *104*, (1), 185-192.
115. Liang, L.; Yang, W.; Guan, X.; Li, J.; Xu, Z.; Wu, J.; Huang, Y.; Zhang, X., Kinetics and mechanisms of pH-dependent selenite removal by zero valent iron. *Water Research* **2013,** *47*, (15), 5846-5855.
116. Ling, L.; Pan, B. C.; Zhang, W. X., Removal of selenium from water with nanoscale zero-valent iron: Mechanisms of intraparticle reduction of Se(IV). *Water Research* **2015,** *71*, 274-281.
117. Bruggeman, C.; Maes, A.; Vancluysen, J.; Vandenmussele, P., Selenite reduction in Boom clay: Effect of FeS2, clay minerals and dissolved organic matter. *Environmental Pollution* **2005,** *137*, (2), 209-221.
118. Charlet, L.; Scheinost, A. C.; Tournassat, C.; Greneche, J. M.; Géhin, A.; Fernández-Martı´nez, A.; Coudert, S.; Tisserand, D.; Brendle, J., Electron transfer at the mineral/water interface: Selenium reduction by ferrous iron sorbed on clay. *Geochimica et Cosmochimica Acta* **2007,** *71*, (23), 5731-5749.
119. Cannière, P.; Maes, A.; Williams, S.; Bruggeman, C.; Beauwens, T.; Maes, N.; Cowper, M., Behaviour of Selenium in Boom Clay. State-of-the-art report. **2010**.
120. Scheinost, A. C.; Charlet, L., Selenite Reduction by Mackinawite, Magnetite and Siderite: XAS Characterization of Nanosized Redox Products. *Environmental Science & Technology* **2008,** *42*, (6), 1984-1989.
121. Schwertmann, U.; Cornell, R. M., Iron oxides in the laboratory. In *Iron Oxides in the Laboratory*, Wiley-VCH Verlag GmbH: 2000; pp i-xviii.
122. Liu, J.; Liang, C.; Zhang, H.; Tian, Z.; Zhang, S., General Strategy for Doping Impurities (Ge, Si, Mn, Sn, Ti) in Hematite Nanocrystals. *Journal of Physical Chemistry C* **2012,** *116*, (8), 4986-4992.
123. Galvez, N.; Barron, V.; Torrent, J., Effect of phosphate on the crystallization of hematite, goethite, and lepidocrocite from ferrihydrite. *Clays and Clay Minerals* **1999,** *47*, (3), 304-311.

124. Bolanz, R. M.; Wierzbicka-Wieczorek, M.; Caplovicova, M.; Uhlik, P.; Gottlicher, J.; Steininger, R.; Majzlan, J., Structural Incorporation of As5+ into Hematite. *Environmental Science & Technology* **2013,** *47*, (16), 9140-9147.
125. Das, S.; Essilfie-Dughan, J.; Hendry, M. J., Fate of adsorbed arsenate during phase transformation of ferrihydrite in the presence of gypsum and alkaline conditions. *Chemical Geology* **2015,** *411*, 69-80.
126. Abraitis, P. K.; Pattrick, R. A. D.; Vaughan, D. J., Variations in the compositional, textural and electrical properties of natural pyrite: a review. *International Journal of Mineral Processing* **2004,** *74*, (1-4), 41-59.
127. Morse, J. W., Interactions of Trace-Metals with Authigenic Sulfide Minerals - Implications for Their Bioavailability. *Marine Chemistry* **1994,** *46*, (1-2), 1-6.
128. Morse, J. W.; Luther, G. W., Chemical influences on trace metal-sulfide interactions in anoxic sediments. *Geochimica Et Cosmochimica Acta* **1999,** *63*, (19-20), 3373-3378.
129. Rickard, D.; Luther, G. W., Chemistry of iron sulfides. *Chemical Reviews* **2007,** *107*, (2), 514-562.
130. Bildstein, O.; Trotignon, L.; Perronnet, M.; Jullien, M., Modelling iron-clay interactions in deep geological disposal conditions. *Physics and Chemistry of the Earth* **2006,** *31*, (10-14), 618-625.
131. De Craen, M.; Van Geet, M.; Wang, L.; Put, M., High sulphate concentrations in squeezed Boom Clay pore water: evidence of oxidation of clay cores. *Physics and Chemistry of the Earth* **2004,** *29*, (1), 91-103.
132. Gaucher, E.; Robelin, C.; Matray, J. M.; Negral, G.; Gros, Y.; Heitz, J. F.; Vinsot, A.; Rebours, H.; Cassagnabere, A.; Bouchet, A., ANDRA underground research laboratory: interpretation of the mineralogical and geochemical data acquired in the Callovian-Oxfordian formation by investigative drilling. *Physics and Chemistry of the Earth* **2004,** *29*, (1), 55-77.
133. Joseph, C.; Schmeide, K.; Sachs, S.; Brendler, V.; Geipel, G.; Bernhard, G., Sorption of uranium(VI) onto Opalinus Clay in the absence and presence of humic acid in Opalinus Clay pore water. *Chemical Geology* **2011,** *284*, (3-4), 240-250.
134. Missana, T.; Alonso, U.; Scheinost, A. C.; Granizo, N.; García-Gutiérrez, M., Selenite retention by nanocrystalline magnetite: Role of adsorption, reduction and dissolution/co-precipitation processes. *Geochimica et Cosmochimica Acta* **2009,** *73*, (20), 6205-6217.
135. Diener, A.; Neumann, T., Synthesis and incorporation of selenide in pyrite and mackinawite. *Radiochimica Acta* **2011,** *99*, (12), 791-798.
136. Diener, A.; Neumann, T.; Kramar, U.; Schild, D., Structure of selenium incorporated in pyrite and mackinawite as determined by XAFS analyses. *Journal of Contaminant Hydrology* **2012,** *133*, 30-39.
137. Francisco, P. C. M.; Sato, T.; Otake, T.; Kasama, T.; Suzuki, S.; Shiwaku, H.; Yaita, T., Mechanisms of Se(IV) Co-precipitation with Ferrihydrite at Acidic and Alkaline Conditions and Its Behavior during Aging. *Environmental Science & Technology* **2018,** *52*, (8), 4817-4826.
138. Börsig, N.; Scheinost, A. C.; Shaw, S.; Schild, D.; Neumann, T., Uptake mechanisms of selenium oxyanions during the ferrihydrite-hematite recrystallization. *Geochimica et Cosmochimica Acta* **2017,** *206*, 236-253.